UCLouvain

École polytechnique de Louvain

Detonation suppression by porous obstacles

Author: **Sacha POUSSEUR**
Supervisor: **Miltiadis PAPALEXANDRIS**
Readers: **Julien CARLIER, Vincent LEGAT**
Academic year 2023–2024
Master [120] in Mechanical Engineering

This page is intentionally left blank

Abstract

The aim of this master's thesis is to investigate numerically the suppression of accidental detonations by highly porous obstacles. Numerical simulations will therefore focus on the compressible flow behavior of a two-phase mixture (gas and solid matrix of the porous medium) based on a thermomechanical model for flows in superimposed fluid/solid regions. Simulations are performed using an algorithm and software written by Prof. Papalexandris' research team.

The results show that in most cases, porous obstacles succeed in decoupling the detonation from the reaction zone, leading to their suppression. This shows that the force exerted by the porous material on the reactive mixture acts as a sink of momentum and kinetic energy. By contrast, a specific configuration of biperiodically arranged blocks, not covering the entire cross-section, does not predict whether detonation is eliminated or not. Nevertheless, the shockwave is weakened by the interphasial force inflicted by the obstacles and, therefore, propagates as a low-speed detonation without quenching.

This page is intentionally left blank

Aknowledgements

Je voudrais exprimer ma sincère reconnaisance envers les personnes qui ont contribué de près ou de loin à la réalisation de ce mémoire, un travail exigeant qui n'aurait pas vu le jour sans leur précieux soutien.

Je tiens d'abord à remercier mon promoteur, Monsieur Miltiadis Papalexandris, pour sa disponibilité constante, ses conseils avisés et ses explications détaillées qui m'ont permis de me familiariser avec les outils nécessaires à ce travail. Son accompagnement à été essentiel tout au long de ce projet.

Je remercie également M. Julien Carlier et M. Vincent Legat pour avoir accepté d'être lecteurs de mon mémoire. Leur temps consacré à cette tâche est grandement apprécié.

Écrire un mémoire en anglais n'a pas été une tâche aisée, je remercie donc fortement Juliette Burton d'avoir pris le temps de relire et de corriger ce travail avec soin.

Enfin, je tiens à remercier ma famille et mes amis pour leur soutien sans faille durant toutes ces années d'études, sans qui rien de tout ça n'aurait été possible. Une mention spéciale va à ma copine, qui n'a jamais cessé de m'encourager, et ce dans toutes les circonstances. Elle a été une réelle source de motivation, et je ne peux que la remercier pour cela.

This page is intentionally left blank

Contents

List of Figures

List of Tables

1 Introduction

The handling, storage, and transportation of high explosives have always involved safety risks, a fact that has been emphasized throughout their history. The discovery of nitroglycerin by the Italian chemist A. Sobrero in 1847, which revolutionized the field of explosives, is a notable example. However, nitroglycerin's intrinsic instability made it extremely dangerous to handle and transport, leading to a series of serious accidents. Among these was the explosion at the A. Nobel's factory, which promped him to create a far more stable substance in 1866 : dynamite.

Of course, the field of explosives has evolved considerably and is no longer as unstable as it once was, but the accidental formation of a detonation wave remains a real risk. Naturally, this is also the case when ignitable gases are used in certain industrial applications, such as hydrogen. Therefore, it is important to develop appropriate mitigation strategies to attenuate and suppress detonations.

1.1. Detonation: mechanism, formation and theoretical models

Detonation is a high-pressure combustion process characterized by supersonic velocities of the reaction zone relative to the reactants. This rapid combustion is initiated and sustained by a precursor shock wave that propagates through a combustible mixture. The latter is generally a fuel-air or fuel-oxygen mixture.

The shock wave compresses the reactants with a sharp rise in temperature and pressure, enabling them to react directly after the shock. This close connection between the shock wave and the reaction zone enables the latter to remain attached to the shock and propagate along with it. An ideal detonation with its pressure and temperature profile is shown in Figure 1.1. Typical propagation speeds of gaseous detonations generally range from 1 to 10 km/s [1, 2].

In most cases, a detonation can be triggered in two different ways [1]. The first is called "direct initiation", where initiation is achieved by adiabatic compression of the combustible mixture. The result is the formation of a shock wave which, as it progresses, raises the temperature and eventually ignites the fuel mixture, creating detonation. The second is called "deflagration-to-detonation transition (DDT)". As its name suggests, this phenomenon occurs during a transition when a subsonic combustion process (deflagration) becomes a supersonic combustion process (detonation). The flame front in a pipe or channel is generally accelerated by conditions of instability that increase the turbulence of the system (such as changes in cross-section, roughness, etc.) accompanied by an increase in flame surface area and thus the rate of combustion. As the deflagration accelerates, pressure waves are created and interact with the flame front. If velocity and pressure increase sufficiently, the shock wave will attach itself to the flame front, establishing the detonation process. Although these events are rare, they are not less dangerous and often lead to large-scale disasters. This is why detonation attenuation remains an important research topic.

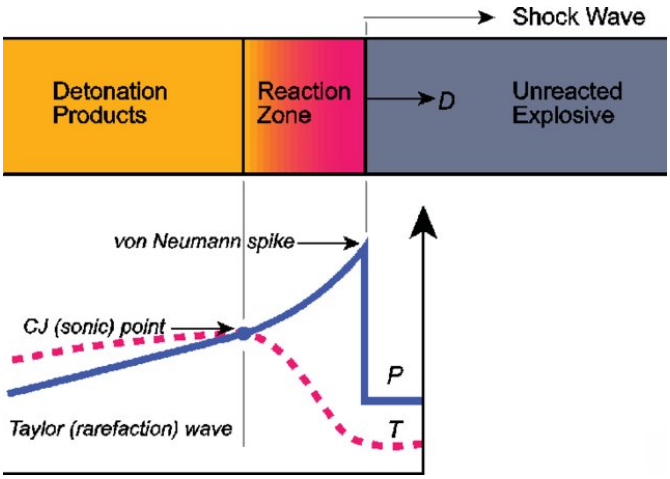

Figure 1.1: Ideal detonation process [3]

One of the earliest theoretical prediction models for gaseous detonations is the Chapman-Jouguet (CJ) theory, which dates back to early 1900s [4, 5]. Based on the assumptions that the reaction zone is infinitely thin and that the detonation wave travels at constant velocity, the CJ condition defines the critical parameters (pressure, temperature, and density) at which the wave can be kept stable [1, 3]. This condition represents the minimum energy required to maintain a detonation wave at a steady state, where the reactants are fully consumed in the reaction behind the detonation wave. At this point, the wave speed is independent from chemical reaction kinetics [6].

In addition to offering simplicity and ease of analysis, CJ theory serves as a fundamental reference for more complex models, providing valuable insights into detonation phenomena.

During World War II, Y. Zeldovich, J. von Neumann, and W. Döring independently developed a model which describes the structure of one-dimensional steady detonation waves assuming finite-rate chemistry : the ZND model [7–9]. Although based on CJ theory, this time the combustion zone is not considered infinitely thin [1]. ZND model assumes a steadily moving shock wave followed by a reaction in a compressible, inviscid and constant-area flow. As can be seen in Figure 1.1, the combustible mixture is compressed to a high pressure and temperature (von Neumann spike). After induction, a highly exothermic reaction begins, and stops at the end of the ZND reaction zone. The products then expand backward, away from the shock front [3].

1.2. Applications and innovations

The interaction between shock waves and chemical reactions enables detonations to achieve considerable efficiency and power, making it a versatile phenomenon with applications ranging from explosives to advanced propulsion systems. Research continues to intensify on the complex subject of shock-induced combustion in order to optimize the various technologies based on detonation. Here are few examples of applications:

- Explosive devices;
- Detonation spraying;
- Explosive manufacturing;

One of these manufacturing technologies is the production of nanodiamonds by detonation. To obtain them, the process involves detonating a mixture of carbon-containing compounds in an atmosphere of N_2, H_2O and CO_2. It is interesting to note that this compound has become an active research topic due to its highly promising properties, particularly in biological, electronic, and quantum physics applications [10].

Some innovative propulsion technologies also use detonation [2], those include:

- Pulsed-Detonation Engine (PDE);
- Rotating-Detonation Engine (RDE);
- Oblique-Detonation Wave Engine (ODWE);

PDEs work by igniting an air/fuel mixture in pulses, creating repeated detonations. Each detonation creates a high-pressure, high-temperature gas that expands, generating thrust. Where PDEs have a cyclic process, RDEs maintain a "continuous" detonation that rotates around an annular combustion chamber. This makes them potentially more efficient engines than PDEs. Finally, ODWEs are expected to operate at even higher speeds. It generates a steady oblique detonation wave that continuously compresses and ignites the air/fuel mixture, making them highly effective for hypersonic propulsion. Their design is shown in Figure 1.2.

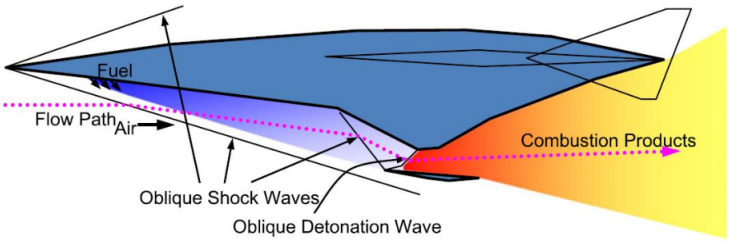

Figure 1.2: ODWE design with formation of oblique shock wave [11]

Having demonstrated the enormous potential of detonation through various applications, it is important to remember that it remains a dangerous phenomenon which requires careful management and control.

This thesis is more focused on safety aspects because, as already mentioned, detonations can have disastrous consequences in the event of accidental formation. The approach of this work therefore focuses on a numerical analysis in mitigating or suppressing detonations.

1.3. State of the art

When it comes to attenuating or suppressing gaseous detonations, different solutions come into play. In the context of shock waves propagating in a channel or a pipe, attenuation methods generally fall into two categories: chemical or mechanical [12]. These approaches aim either to modify the chemical composition of the gas mixture or to manipulate the physical geometry of the duct to disrupt the propagation of the detonation wave. By taking advantage of these various strategies, it is possible to effectively mitigate the destructive potential of detonations.

1.3.1. Attenuation by chemical means

In most studies on this subject, detonation attenuation is investigated through the influence of chemical inhibitors or diluents [13–16].

Chemical inhibitors

Inhibitors are in most cases halogenated compounds, which are already known for their ability to extinguish flames. They are able to interfere with the chemical reactions involved in the detonation process, which can slow down or interrupt the radical chain reactions that propagate combustion.

F. Evariste et al. [14] have shown that the effectiveness of inhibition depends on the type of radicals involved, with H radicals being more effective than OH or O radicals. Inhibition capacity is also influenced by the rate coefficient of the individual elementary inhibition reaction. Their research also revealed that bromine-containing compounds, in particular CF_2HBr, are the most effective, while chlorine-containing species require higher quantities. CF_3H has no inhibiting effect but can cause detonation failure at high concentrations by genuine thermal effect. Overall, bromine atoms are essential for effective chemical inhibition in hydrogen-rich fuels.

Diluents

Concerning diluents, inert gases such as nitrogen, carbon dioxide, or argon can be added to the mixture to dilute explosive gases. The idea is to reduce the concentration of reactive compounds, so that there is not enough "fuel" present for combustion to occur.

In a study by Zhang et al. [16], the dynamic detonation parameters of stoichiometric mixtures of acetylene and oxygen diluted with varying amounts of argon were measured and analyzed. Their results revealed that the critical tube diameter and the critical energy required to directly initiate spherical detonations increased with argon dilution.

1.3.2. Attenuation by mechanical means

Mechanical means are generally divided into two different types : detonation diffraction or the insertion of one or more solid obstacles.

Detonation diffraction

Numerous studies have focused on the phenomenon of detonation diffraction [17–21]. A detonation wave traveling through a channel diffracts when it encounters a widening. This specific widening causes a bending of the detonation front, which can lead to the decoupling of the main shock wave from the reaction zone and

potentially to the extinction of the detonation.

In most articles cited above, simulations predict three types of detonation evolution: supercritical, critical and subcritical [17, 18, 20]. In the case of supercritical detonation, the zone of reaction is constantly attached to the precursor shock, whereas in the case of critical detonation, it is momentarily detached before being reattached to the front. In a subcritical detonation, the reaction zone permanently detaches, leading to detonation quenching. More specifically, Papalexandris et al. [17] presented numerical simulations examining the evolution of two-dimensional detonation waves as they spread from a narrow channel to a wider one. The effects of fuel activation energy and channel width ratio were examined by means of a parametric study. Their results show that sufficiently high values of these parameters can lead to critical or even subcritical flows.

On the left, Figure 1.3 shows a schematic of this phenomenon : the detonation cells disappear from the channel wall towards the axis of the system, following a path known as the extinction cone. The right side is a coupled part of the reaction zone surrounded by a decoupled part after diffraction in the subcritical regime.

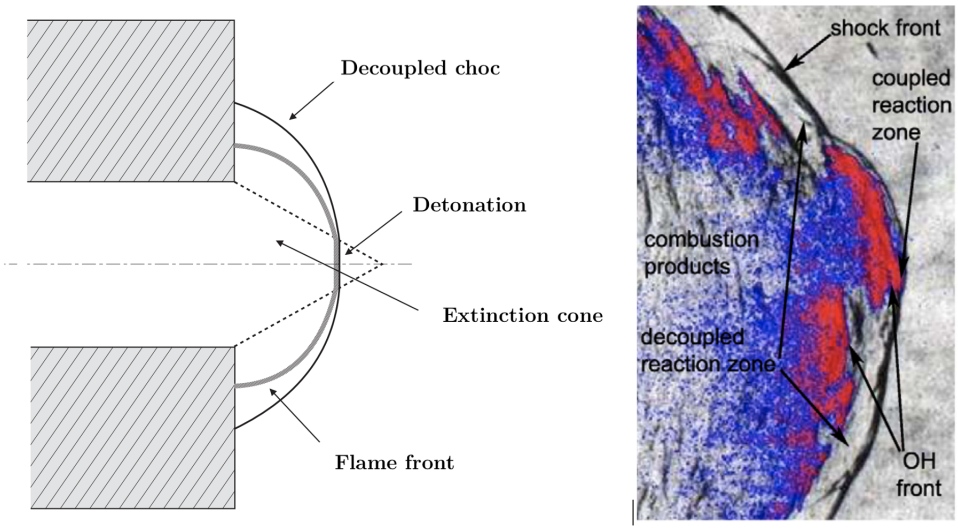

Figure 1.3: Left: Schematic diagram of detonation diffraction; Right: Enlarged portion of a planar laser-induced fluorescence image in a sub-critical regime, P0 = 100 kPa [18]

This diffraction can take place through various geometric configurations: a sharp increase in width, as shown in Figure 1.3 (left), but also conical divergences with different angles, etc.

Solid obstacles

Solid obstacles have also been extensively studied in the context of detonation waves [12]. This is of particular interest here, as it is the main focus of this master's thesis. The key factor in the attenuation of detonation by these obstacles is the force they exert on the reactive mixture, which acts as a sink for momentum and kinetic energy. This force reduces the intensity of the shock wave, thus weakening detonation.

Over the years, researchers have explored a wide variety of obstacles and configurations, experimenting with different materials and shapes. In most cases, the resulting detonations propagate at lower velocities than their Chapman-Jouguet equivalents. These are known as quasi-detonations. The propagation mechanisms of quasi-detonations have been studied in several ways:

- *Theoretically*, Dionne et al. [22] investigated these low velocity detonations (LVD) in tubes with dense obstacle arrays, using a friction factor to account for momentum loss. Although the generalized C-J criterion can predict stable detonation structures, it fails below a certain velocity. In fact, they remarked that there is no steady-state solution for high friction values that leads to LVD. Other theoretical frameworks were examined, such as Zeldovich's quasi-one-dimensional model discussed in the article by I. Brailovsky and G. Sivashinsky [23].

- *Numerical simulations* have also been carried out to study the re-ignition mechanism of detonations. In particular, Medvedev et al. [24] have studied this phenomenon through apertured obstacles for a gaseous mixture of hydrogen and air. They noticed that the detonation dissipated in contact with the obstacle, forming unstable streams of detonation products. The reflection of the precursor shock from the domain walls then heats the unburnt material, causing an accelerating deflagration that eventually reattaches to the front, leading to the re-initiation of the detonation.

- Finally, the *experimental results* are close to those obtained numerically by Medvedev et al. The findings of Teodorczyk et al. [25] indicate that quasi-detonation propagation mechanisms appear to be caused by re-initiation via reflection of shocks on the walls. Based on this observation, they underline an important point: "it is not clear that the ignition itself is a consequence of adiabatic shock heating or vortex mixing in the wall jet shear layer zone near the wall behind the Mach stem".

Regarding porous objects in particular, numerous studies have also been carried out. Porous obstacles can be considered as a set of densely spaced objects. As early

as 1984, G. A. Lyamin [26] used quartz sand in his experiment. The problem is that it is difficult to define specific properties for a medium whose shapes and sizes vary widely. Consequently, it wasn't possible to relate the propagation velocity to the morphological details of the porous medium. Instead, experiments were carried out with spheres or cylinders of different sizes and materials, such as ceramic, steel, or glass [27–29]. These studies highlighted a significant loss of momentum and the transition to quasi-detonation induced by porous obstacles. They also provided a better understanding of the detonation re-initiation mechanism downstream of the porous medium.

More recently, other porous coatings were studied, such as polyurethane foam (95% porosity) or steel wool (99% porosity). These experiments, carried out by Bivol et al. [30], analyzed the attenuation of detonations from a hydrogen-air mixture in rectangular-section channels lined with these porous substances. In both cases, the detonation wave decoupled into a shock wave and a subsonic flame, close to the CJ acoustic velocity. At the end of the porous section, the shock pressure was reduced by 70% for polyurethane foam and 85% for steel wool. They then continued their research by studying other parameters such as the pore size of the polyurethane foam, or even sections of different sizes [31, 32].

1.3.3. Reference paper

In many of the papers mentioned in the previous subsection, the volumetric momentum sink is represented by a constant coefficient of friction. This prevents spatial variations in porosity, and hence multidimensional flows, from being taken into account. Furthermore, in all of these papers, the porous elements of the solid matrix are considered to be at least as large as the length of the reaction zone.

However, a study by M.V. Papalexandris [12] has overcome these limitations by using detailed numerical simulations to model the transmission of detonation in channels both in 1D and 2D. His approach provides an accurate representation of the flow structure and detonation re-initiation mechanisms in the presence of porous media with variable porosity and finer microstructures.

This master's thesis builds on and extends the research carried out by Prof. Papalexandris in the article "*Attenuation of gaseous detonations by porous media of fine microstructure*" [12]. As the present paper uses the same mathematical and physical model as in his study, it is important to review every aspects of his approach. Here is a summary of the key elements used:

– **Fine microstructure** – The porous materials under consideration have very high porosity: the fiber diameter of the matrix is inferior to the characteristic chemical length scale.

– **Thermo-mechanical model** – The study is based on a thermomechanical model for flows in superimposed regions of pure fluids and porous media. According to this model and due to the fine microstructure, porous obstacles are modeled as rigid solid continuums and their porosity is introduced as a constant-time but spatially varying field variable.

– **Chemical kinetics** – For chemical kinetics, two three-step branching mechanisms were analyzed. One is suitable for high-pressure conditions, the other for low to moderate pressures.

These aspects will be reviewed in much more details in the next section. The simulations ran in the frame of the study have led to the following observations:

– **Re-initation and suppression** – With a single porous section, detonation is significantly attenuated, but re-initiate downstream via a chain explosion. In contrast, arrays of porous sections covering the entire channel cross-section decouple the reaction zone from the main shock wave, ensuring effective detonation suppression.

– **Low-velocity detonations** – In domains with networks of porous blocks that only partially cover the channel cross-section, detonations do not extinguish but propagate as low-velocity detonations.

Based on these hypotheses and methodologies, this research aims to further elucidate the mechanisms of detonation suppression using porous obstacles, which could contribute to the development of more effective detonation arresting devices. To this end, this paper is structured as follows:

First, Chapter 2 develops the mathematical model on which the simulations are based. It is in fact a thermomechanical model that links superimposed fluid and porous regions. To this end, equilibrium laws for the gas phase and the solid phase are developed to obtain a numerically solvable system.

Before solving the system, Chapter 3 explains the calculation setup. The algorithm is based on a FORTRAN code that enables 1D and 2D simulations to be carried out. First, the algorithm is explained in more detail and the calculation domain is introduced; then all the required parameters for correct operation are set.

Chapter 4 presents all the simulation results obtained in 1D and 2D. These are interpreted and compared with each other and important results are highlighted. Other articles are also mentioned for comparison.

Finally, Chapter 5 concludes this master's thesis and summarizes all the results obtained throughout the course of this research. It also suggests ways in which this work and these studies can be extended.

2 Mathematical model

As explained previously, the mathematical model that have been used for the numerical study is the same as in M.V. Papalexandris' paper [12]. This thermo-mechanical model [33] is based on the same mixture theory formalism as in the article "A two-phase model for compressible granular flows based on the theory of irreversible processes" [34]. In this approach, the fluid and solid phases (porous region) are treated as two coexisting but open thermodynamic continua, interacting with each other. The latter involves heat transfer and interphasial mass exchange.

In the model under consideration, the porous obstacle material is assumed to be a rigid, chemically inert solid with constant mass density and zero velocity. Similarly, the study assumes that the solid matrix does not undergo any phase change. Porosity is then expressed as in most two-phase continuum theories, i.e. as a distribution that measures the volume density occupied by the fluid along the physical space: $\phi(x)$. It can then be expressed as a volume ratio that remains constant over time:

$$\phi(x) = \frac{\mathrm{d}V_f}{\mathrm{d}V} \tag{2.1}$$

where V_f represents the volume taken by the fluid, and V is the physical domain volume. In addition, $\phi(x)$ is considered as a continuous function. Therefore, the boundaries between porous and pure fluid regions are not abrupt, but are assumed to be smooth and to possess a finite thickness. This feature enables practical numerical modeling, as interface thicknesses can be adjusted as required. As a result, the density inside the solid matrix gradually decreases to zero instead of undergoing a sudden drop. This smooth transition results in more accurate and more manageable simulations.

The two thermodynamic systems of fluid and solid matrix are open and not in equilibrium. This means they can interact with each other, involving the exchange of mass, momentum and energy.

2.1. Gaseous phase balance laws

Now that porosity distribution has been explicitly detailed, it is necessary to review the assumptions and specific parameters before introducing the balance laws of mass, momentum and energy for the gaseous phase:

- The reactive gas mixture comprises three primary species : reactants F, radicals R and combustion products P. For the sake of simplicity, these species are considered as perfect gases with the same heat capacity ratio γ ;
- The heat diffusion and viscous dissipation are assumed negligible for the gas mixture ;
- The momentum exchange between fluid and porous phases is written as $\boldsymbol{f}$, and is expressed as :

$$\boldsymbol{f} = p\nabla\phi - \boldsymbol{\beta} \cdot \boldsymbol{u} \tag{2.2}$$

  where p is the pressure, $\boldsymbol{u}$ is the velocity vector, and $\boldsymbol{\beta}$ is a matrix that represents the interphasial drag parameter. In this case, the porous material is considered orthotropic[1];
- Interphasial heat exchange is represented as $\mathcal{E}$:

$$\mathcal{E} = h(T - T_s) \tag{2.3}$$

  where h is the coefficient of interphasial heat exchange, T is the gas temperature and T_s is the porous matrix temperature.

Having done this, here are the dimensionless mass, momentum, and energy balances, in a simplified form:

$$\frac{\partial}{\partial t}(\phi\rho) + \nabla \cdot (\phi\rho\boldsymbol{u}) = 0 \tag{2.4}$$

$$\frac{\partial}{\partial t}(\phi\rho\boldsymbol{u}) + \nabla \cdot (\phi\rho\boldsymbol{u}\boldsymbol{u}) + \nabla(\phi p) = \boldsymbol{f} \tag{2.5}$$

$$\frac{\partial}{\partial t}(\phi\rho e_t) + \nabla \cdot (\phi(\rho e_t + p)\boldsymbol{u}) = \boldsymbol{f} \cdot \boldsymbol{u} + \mathcal{E} \tag{2.6}$$

where ρ represents the mass density.

[1]"A material is orthotropic if its mechanical or thermal properties are unique and independent in three mutually perpendicular directions" [35]

Since F, R and P are perfect gases with the same heat capacity ratio, the ideal gas law can be written as $p = \rho T$. Therefore, according to equation (2.6), the total energy of the gaseous phase e_t can be expressed as the sum of the internal, kinetic and thermal energy:

$$e_t = \frac{1}{\gamma - 1}\frac{p}{\rho} + \frac{1}{2}\boldsymbol{u} \cdot \boldsymbol{u} + q(Y_\mathrm{F} + Y_\mathrm{R}) \tag{2.7}$$

with q the heat released by combustion and Y_F, Y_R the mass fraction of the reactants and the radicals, respectively. The term $(\gamma - 1)$ appears due to the relations of the heat capacity ratio $\gamma = \frac{c_p}{c_v}$ and the expression of the specific gas constant $R = c_p - c_v$, with c_p and c_v the specific heat at a constant pressure and volume respectively.

In addition, the species concentration laws are expressed as follows:

$$\frac{\partial}{\partial t}(\phi\rho Y_i) + \nabla \cdot (\phi\rho\boldsymbol{u}Y_i) = \dot{\omega}_i, \qquad i = \mathrm{F},\, \mathrm{R},\, \mathrm{P} \tag{2.8}$$

where Y_i is the mass fraction of the different species F, R and P, and ω_i denotes the source term resulting from the chemical reactions in which the species are involved. Since the sum of the mass fractions of the various components is exactly 1 ($Y_\mathrm{F} + Y_\mathrm{R} + Y_\mathrm{P} = 1$), the system (2.8) requires only two of the three equations to be solved.

The system of equations from (2.4) to (2.6) as well as (2.8) can be expressed more comprehensively by introducing momentum exchange $\boldsymbol{f}$ (2.2) and interphasial heat exchange $\mathcal{E}$ (2.3), while noting that porosity $\phi(x)$ does not depend on time. It is then possible to obtain the left-hand side of the system similar to Euler's compressible equations:

$$\frac{\partial \rho}{\partial t} + \nabla \cdot (\rho\boldsymbol{u}) = -\frac{\rho}{\phi}\boldsymbol{u} \cdot \nabla\phi \tag{2.9}$$

$$\frac{\partial \rho\boldsymbol{u}}{\partial t} + \nabla \cdot (\rho\boldsymbol{u}\boldsymbol{u}) + \nabla p = -\frac{\rho}{\phi}(\boldsymbol{u}\boldsymbol{u}) \cdot \nabla\phi - \frac{1}{\phi}\boldsymbol{\beta} \cdot \boldsymbol{u} \tag{2.10}$$

$$\frac{\partial \rho e_t}{\partial t} + \nabla \cdot ((\rho e_t + p)\boldsymbol{u}) = -\frac{\rho e_t}{\phi}\boldsymbol{u} \cdot \nabla\phi - \frac{1}{\phi}(\boldsymbol{\beta} \cdot \boldsymbol{u}) \cdot \boldsymbol{u} + \frac{h}{\phi}(T - T_s) \tag{2.11}$$

$$\frac{\partial \rho Y_j}{\partial t} + \nabla \cdot (\rho\boldsymbol{u}Y_j) = -\frac{\rho Y_j}{\phi}\boldsymbol{u} \cdot \nabla\phi + \frac{\dot{\omega}_j}{\phi}, \qquad j = \mathrm{F},\, \mathrm{R} \tag{2.12}$$

As porosity $\phi(x)$ is a fixed variable for the numerical simulations, it is assumed to be known. This implies that the terms on the right-hand side that take into account the porosity gradient $\nabla\phi$ act as source terms rather than as nonconservative

products. In this case, this represents a big advantage, since the system will remain strictly hyperbolic and will share the same eigenvalues and eigenvectors as the compressible Euler equations. This property generally guarantees the existence and uniqueness of solutions, which simplifies the numerical resolution of the system. The process would be much more complex if the products on the right-hand side were nonconservative[2]. The system therefore produces distinct and real solutions that will be obtained numerically using shock-capturing algorithms for hyperbolic conservation laws with source terms, developed as part of Prof. Papalexandris's paper [12] by a team of researchers from his department.

2.2. Porous matrix balance laws

The equilibrium laws for the porous matrix are different from those for the gaseous mixture. As mentioned above, the porous material is assumed to be a rigid, chemically inert solid with a constant mass density and zero velocity. This means that both sides of the balance laws of mass and momentum become identically equal to zero. This leaves the energy balance equation, which can be expressed as :

$$(1-\phi)\rho_s c_s \frac{\partial T_s}{\partial t} = -(\gamma-1)\mathcal{E} \tag{2.13}$$

with ρ_s, c_s and T_s respectively the density, specific heat capacity and temperature of the solid matrix. Again, the term $(\gamma-1)$ comes from the fact that both sides are nondimensionalized. Since solving this equation is simpler than for gas equilibrium, a second-order Runge-Kutta (RK2) solver is used.

2.3. Fluid-solid complete system

By now, the equations from (2.9) to (2.13) are all nondimensionalized by the reference variables in a nonreacting case. By non-reacting case, the reference article of this model [33] means that the non-dimensionalizations of the coefficients and variables are realized by the reference values **ahead** of the shock. For example, the pressure, temperature, and density are non-dimensionalized by the reference values p_0, T_0, and ρ_0, respectively. In addition, the reference velocity u_r is defined by $u_r = \sqrt{\frac{p_0}{\rho_0}}$.

[2]"In particular, these terms do not permit the balance equations to be written in conservative (divergence) form in the hyperbolic limit. (That is, in the limit where viscosity and other dissipative terms are zero.) As a result, weak solutions of these equations can not be defined in the standard sense of distributions."[36]

The final system below brings together all the balance laws for the fluid and solid phases:

$$\frac{\partial \rho}{\partial t} + \nabla \cdot (\rho \boldsymbol{u}) = -\frac{\rho}{\phi} \boldsymbol{u} \cdot \nabla \phi \tag{2.14}$$

$$\frac{\partial \rho \boldsymbol{u}}{\partial t} + \nabla \cdot (\rho \boldsymbol{u}\boldsymbol{u}) + \nabla p = -\frac{\rho}{\phi} (\boldsymbol{u}\boldsymbol{u}) \cdot \nabla \phi - \frac{1}{\phi} \boldsymbol{\beta} \cdot \boldsymbol{u} \tag{2.15}$$

$$\frac{\partial \rho e_t}{\partial t} + \nabla \cdot ((\rho e_t + p) \boldsymbol{u}) = -\frac{\rho e_t}{\phi} \boldsymbol{u} \cdot \nabla \phi - \frac{1}{\phi} (\boldsymbol{\beta} \cdot \boldsymbol{u}) \cdot \boldsymbol{u} + \frac{\mathcal{E}}{\phi} \tag{2.16}$$

$$\frac{\partial \rho Y_j}{\partial t} + \nabla \cdot (\rho \boldsymbol{u} Y_j) = -\frac{\rho Y_j}{\phi} \boldsymbol{u} \cdot \nabla \phi + \frac{\dot{\omega}_j}{\phi}, \qquad j = \mathrm{F},\, \mathrm{R} \tag{2.17}$$

$$(1 - \phi) \rho_s c_s \frac{\partial T_s}{\partial t} = -(\gamma - 1) \mathcal{E} \tag{2.18}$$

A final clarification concerns the assumption made about the porosity distribution $\phi(x)$. The continuum hypothesis used in this model only applies when the micro-elements composing the porous material have diameters much smaller than the characteristic length scales of the flow. For the scope of the present research, it is therefore ensured that this statement is respected. This ensures that microscopic details do not significantly affect the macroscopic behavior of the system, enabling the model to effectively capture global exchanges of momentum and energy, as well as the impact of porosity gradients.

2.4. Chemical kinetics

The kinetic reaction model used in this work is a three-step chain branching reaction. It includes a chain initiation phase and a chain branching phase, both governed by Arrhenius kinetics [37]. There are then two different termination phases: termination I and II. The primary species involved are the same as those presented above, with one exception: a fourth inert species, M, is added for the second termination as illustrated in the following chain-branching schemes :

$$\text{Chain-initiation :} \qquad \mathrm{F} \xrightarrow{\mathrm{k_i}} \mathrm{R}, \qquad k_i(T) = A_i e^{-\frac{E_i}{T}} \tag{2.19}$$

$$\text{Chain-branching :} \qquad \mathrm{F} + \mathrm{R} \xrightarrow{\mathrm{k_b}} 2\,\mathrm{R}, \qquad k_b(T) = A_b e^{-\frac{E_b}{T}} \tag{2.20}$$

$$\text{Chain-termination I :} \qquad \mathrm{R} \xrightarrow{\mathrm{k_{t_I}}} \mathrm{P}, \qquad k_{t_I}(T) = A_{t_I} e^{-\frac{E_{t_I}}{T}} \tag{2.21}$$

$$\text{Chain-termination II :} \qquad \mathrm{R} + 2\,\mathrm{M} \xrightarrow{\mathrm{k_{t_{II}}}} \mathrm{P} + 2\,\mathrm{M}, \qquad k_{t_{II}}(T) = A_{t_{II}} e^{-\frac{E_{t_{II}}}{T}} \tag{2.22}$$

with A_x being the pre-exponential factors that set the time scales and E_x the activation energy parameters.

To show the difference between the two terminations (tI and tII), the following table explains the specific conditions favored according to "Combustion and Fuels" [38], along with a description of each case:

Mechanism	**Conditions**	**Description**
tI	High pressure	The key step in termination is the destruction of radicals on the walls.
tII	Low to moderate pressure	The key termination step takes place mainly via collisions between the R radicals and the inert M species.

Table 2.1: Summary of the two different termination mechanisms

In the reactant concentration law equation (2.8), the source term $\dot{\omega}_F$ will be the same for both chain reaction terminations :

$$\dot{\omega}_F = -\rho\phi(Y_F k_i + \rho Y_F Y_R k_b) \tag{2.23}$$

However, for radicals, the expressions for the two terminations are different. The source term for the first mechanism tI is expressed as follows:

$$\dot{\omega}_{R_{tI}} = \rho\phi(Y_F k_i + \rho Y_F Y_R k_b - Y_R k_{tI}) \tag{2.24}$$

For the second mechanism tII, it is expressed as :

$$\dot{\omega}_{R_{tII}} = \rho\phi(Y_F k_i + \rho Y_F Y_R k_b - \rho^2 Y_R k_{tII}) \tag{2.25}$$

By examining the right-hand sides of equations (2.24) and (2.25), it can be concluded that the rate of the termination reaction tI is linearly related to density ρ, while the rate of the termination reaction tII is quadratically related to ρ.

3 Computational setup

The FORTRAN algorithm written by the research team allows 1D and 2D simulations to be carried out with a domain partially filled with a porous matrix. In this chapter, this algorithm is explained in more detail along with its application domain. All the variables required for its correct operation are also introduced, and fixed where necessary.

3.1. Algorithm scheme

To solve the gas-phase equations from (2.14) to (2.17), a shock-capture algorithm for hyperbolic conservation laws with source terms has already been mentioned in the previous chapter. This algorithm comes from the papers by M. V. Papalexandris, A. Leonard and P. E. Dimotakis [39, 40].

The algorithm is of the MUSCL (Monotonic Upstream-centered Scheme for Conservation Laws) type, designed for the numerical study of multidimensional systems of hyperbolic conservation laws with source terms, such as the compressible Euler equations for reactive flows, as is the case here. This is a fully unsplit shock capture scheme, meaning that it avoids dimensional and temporal splitting by integrating all terms of the governing equations simultaneously in a single time step.

The algorithm works by decomposing the governing system into a set of ordinary differential equations (ODEs) that are satisfied along the characteristic trajectories of the corresponding homogeneous one-dimensional problem [39]. These equations are valid along specific space-time manifolds, called Riemann invariant manifolds. The local geometry of these manifolds depends on the source terms and spatial derivatives of the flow variables. The numerical integration of these characteristic equations is performed during the ascent step of the algorithm.

In summary, this algorithm is notable for its ability to simultaneously integrate conservation equations in multi-dimensional systems without resorting to temporal or dimensional slicing, using specific spatio-temporal manifolds to accurately capture shock wave dynamics.

As for the solid matrix energy equation (2.18), it is solved by a more conventional method given its simplicity: a second-order Runge-Kutta (RK2) solver.

3.2. Computational domain

First, the length is nondimensionalized as a half-reaction length $l_{1/2}$. This corresponds to the length between the von Neumann spike (where combustion starts right behind the shock) and the point where the mass fraction of radicals is halved ($Y_R = 0.5$).

Regarding the resolution of the grid, it is different for the 1D and 2D simulations:

– In 1D, the grid resolution is 50 points per half-reaction length $l_{1/2}$;

– In 2D, the grid resolution is reduced to 20 points per half-reaction length $l_{1/2}$.

Indeed, the resolution for 2D simulations had to be reduced so that the computer could support the calculations performed. Despite this, the resolution is still acceptable for relevant results and for capturing accurate flow structures.

Furthermore, boundary conditions are set according to the simulations carried out. For all simulations, the left-hand boundary is set with the inflow condition, while the right-hand boundary is set with the outflow condition. The flow direction is therefore always from left to right in the domain. For the top and bottom, there are two types of condition: periodic and reflective. The first is adapted for simulations involving a single porous section or periodic blocks of porous obstacles. The second is designed for simulations requiring wall conditions, such as porous coatings covering the domain walls.

For this specific study, the ZND detonation model was used as the initial condition for all simulations. It has the advantage of being well known and long-established for numerical applications. The ZND wave profile is placed just in front of the porous obstacles for all 1D and 2D simulations. This wave position is located $3l_{1/2}$ downstream of the flow inlet boundary (on the left), while the porous obstacles are positioned $5l_{1/2}$ from the flow inlet, except for one case involving two layers of porous matrix bonded to the walls.

3.3. Initial variables

As explained above, the ZND detonation model was used as the initial condition for all simulations. As highlighted in "Gas Dynamics" university course [1], "it is important to mention that for a wide range of reaction parameters the resulting ZND waves are unstable to small perturbations. In general, only high overdriven detonations are stable". This is why the studied detonations are overdriven. The overdrive factor f can be introduced as:

$$f \overset{\text{def}}{=} \left(\frac{D}{D_{\text{CJ}}}\right)^2 \tag{3.1}$$

with D the detonation speed and D_{CJ} its corresponding Chapman-Jouguet velocity.

For the purposes of this research, a single overdrive factor is used: $f = 1.1$. Then, two different configurations come into play depending on chemical kinetics:

– tIf1.1, which corresponds to the termination reaction I.

– tIIf1.1, which corresponds to the termination reaction II.

In addition, other parameters were set to obtain all initial values required for the simulations.

First, there are the physical parameters of gas, namely the heat capacity ratio, which is set at $\gamma = 1.2$, and the heat of combustion q_0, which is the difference between the enthalpy of formation of the reactants and that of the products:

$$q_0 = h_R^f - h_P^f$$

The value is set at $q_0 = 3$, which is a particularly low value, but which corresponds to fairly well-diluted $H_2/O_2/Ar$ mixtures. As M. Papalexandris points out in his paper [12], this choice is justified, as the effect of the porous obstacle should be more noticeable in a dilute mixture. In addition, the detonation velocity in a diluted mixture is more moderate, which translates into a shorter calculation range, thus saving computation time. The values are summarized in Table 3.1 below.

Physical parameters of the gas	
Parameter	Value
γ	1.2
q_0	3.0

Table 3.1: Summary of the physical parameters of the gas

Next, reaction parameters such as activation energies (E_i, E_b and E_t) and corresponding pre-exponential factors (A_i, A_b and A_t) are also fixed. The dimensionless

values of the activation energies of the chemical reactions are quite low compared to what is typically encountered (see Table 3.2). This is again due to computational simplicity, which can be justified by assuming preheated reactants.

From these values, it is possible to obtain the cross-over temperature T_c, the post-shock temperature T_p, and finally the detonation velocity D for the two cases studied. These are also summarized in Table 3.2. The cross-over temperature T_c is the point at which the rates of branching and termination reactions become equal. As explained by M. Short and J. J. Quirk [41], if the temperature falls below this point, branching reactions slow down relative to termination reactions, thus suppressing ignition over time. For the tIf1.1 detonation case, the post-shock temperature T_p is slightly lower than T_c, making this detonation susceptible to extinction. However, in 1D simulations of this ZND wave, the detonation exhibits multi-mode instabilities but does not extinguish; instead, it propagates in a pulsed mode because the region of high radical concentration remains above T_c, keeping branching reactions faster than termination reactions. This case was selected because the effect of porous obstacles is likely to be more prominent in near-extinction detonations. The other case, tIIf1.1, also features longitudinal instabilities and pulsating propagation, but their post-shock temperatures T_p remain higher than T_c. Table 3.2 shows a summary of the reaction parameters :

Reaction parameters		
Parameter	tIf1.1	tIIf1.1
f	1.1	1.1
A_i	20000	37000
A_b	100000	185000
A_t	3.0	1.4
E_i	20.0	20.0
E_b	15.0	15.0
E_t	0	0
T_c	1.44	1.27
T_p	1.4	1.4
D	2.28	2.28

Table 3.2: Summary of the reaction parameters

Then, as mentioned above, the equations are non-dimensionalized in terms of reference values, i.e. the values of the gas upstream of the shock for pressure, temperature and density (p_0, T_0 and ρ_0 respectively). The reference velocity is then expressed as $u_r = \sqrt{\frac{p_0}{\rho_0}}$. The same applies to the length $l_{1/2}$, which has already been introduced. Finally, the reference time scale is equal to $t_{1/2} = \frac{l_{1/2}}{u_r}$.

As far as the porous matrix is concerned, the various parameters for defining it are also the same as in M. Papalexandris' article [12]. In order to inspire the drag and interphasial heat transfer parameterizations, the solid matrix of porous obstacles is represented by identical, very fine, randomly distributed cylinders. These cylinders are assumed to be parallel to each other and to stand upright, perpendicular to the lower boundary of the domain under study. As explained in the thermomechanical model on which this study is based [33], the drag parameter β_{11} in the direction of flow is approximated as follows; first, the drag per unit length for a 2-dimension flow around a single cylinder is determined. Then it is multiplied by the height of the cylinder l and the number of cylinders per unit area N_s :

$$N_s = \frac{4(1-\phi)}{\pi d_c^2 l}$$

with d_c the diameter of a cylinder, fixed here at $d_c = 0.05 l_{1/2}$. This gives the expression of the drag parameter β_{11} (dimensionless form):

$$\beta_{11} = \frac{2}{\pi} C_D \frac{(1-\phi)}{d_c} |u|$$

where u represents the component of fluid speed in the direction of flow. The literature provides various formulas for determining the drag coefficient C_D of circular cylinder arrays, often based on the porosity of the medium and specific Reynolds number ranges (see article by Sonnenwald et al [42]). For the flows studied here, and for the sake of simplicity, the value is fixed at $C_D = 1$, which corresponds to the drag coefficient of a single cylinder in the expected Reynolds number Re range.

The approach to estimating the interphasial heat transfer parameter h follows the same logic as the one used for the interphasial drag parameter. In concrete terms, the formula for the steady-state heat transfer at the surface of a single cylinder is multiplied by the number of cylinders per unit area previously expressed, N_s. The result is the following non-dimensional expression :

$$h = \frac{4(1-\phi)}{d_c^2} \frac{Nu_{d_c}}{PrRe} \kappa$$

with κ the thermal conductivity of the gas. In this expression, Nu_{d_c} represents the Nusselt number on a microscopic scale, averaged for an individual cylinder. In contrast, Reynolds and Prandtl numbers are determined from reference values on a macroscopic scale. For the Nusselt number, an empirical correlation which is applicable for $Pr \geq 0.73$ is employed :

$$Nu = CRe^m Pr^{\frac{1}{3}}$$

with C and m parameters that are listed in the "Fundamentals of heat and mass transfer" [43]. In the context of this work, interphasial heat exchange has very little impact on the simulations. This is because the conductivity κ of the gas is low and the Reynolds number Re chosen is high (turbulent flow pattern). The influence of detonation attenuation is therefore mainly mechanical. It is also important to mention that these parametrizations for drag and heat transfer are mainly approximate and do not take into account certain factors, such as unsteady flow or cylinder height. However, these approximations are considered sufficient for this study, given its focus on a general orthotropic porous medium.

Finally, there are a few physical parameters related to the porous matrix. To represent the density of the fibers making up the porous matrix, metal wool of density $\rho_s = 6800\rho_0$ was chosen. It has a specific heat of $c_s = 2.2R$, with R being the gas constant of the reactants. The final fixed parameter is the Courant number[1], which is a critical parameter for ensuring the stability of numerical solutions. It is here fixed at $C = 0.7$. Most of the above values are summarized in Table 3.3.

Physical parameters of the matrix	
Parameter	Value
d_c	0.05 $l_{1/2}$
C_D	1.0
Re	3250.0
Pr	0.73
ρ_s	6800 ρ_0
c_s	2.2 R
C	0.7

Table 3.3: Summary of the physical parameters of the porous matrix

[1]"The Courant number can be used in computational fluid dynamics (CFD) simulations to evaluate the time step requirements of a transient simulation for a given mesh size and flow velocity and is linked to the Courant–Friedrichs–Lewy (CFL) stability condition of numerical schemes" [44]

4 Numerical results

The main variable studied in this study is the porosity ϕ ranging from $\phi = 90\%$ to $\phi = 98\%$. It is studied in various 1D and 2D simulations, and in different obstacle configurations. Among the different obstacle configurations, there is first a periodic arrangement that fills the entire cross-section of the domain under study. Then, in 2D, a biperiodic network of porous blocks is analyzed, followed by a separate case where the channel walls are longitudinally covered with a porous coating.

The main purpose of studying porosity in this work is to see which materials would be most suitable in the different configurations analyzed, as well as to compare them and deduce emerging differences between them. With regard to the different configurations, the aim is to analyze the detonation behavior in each of them, and to assess their effectiveness.

4.1. One-dimensional results

A configuration containing a single porous section over the entire cross-section has already been studied in detail in the reference document [12]. Instead, a periodic configuration of these porous obstacles covering the entire cross-section is studied here.

4.1.1. Periodic array of porous sections

Although this configuration is supposed to be two-dimensional, in this particular case the flow remains predominantly one-dimensional. Indeed, with porous sections, lateral instabilities seem to be suppressed, so that the flow behaves as if it were only 1D.

The array is composed of porous obstacles with a thickness of $10l_{1/2}$, distributed periodically every $20l_{1/2}$ and occupying the entire cross-section of the domain. The first obstacle is placed at a distance of $5l_{1/2}$, as stated in the previous section. The first termination reaction tIf1.1 is studied here to evaluate the attenuation of the detonation. As a reminder, the upper and lower boundary conditions are set to periodic. First, a graph of the shock pressure p_s as a function of time is presented on Figure 4.1.

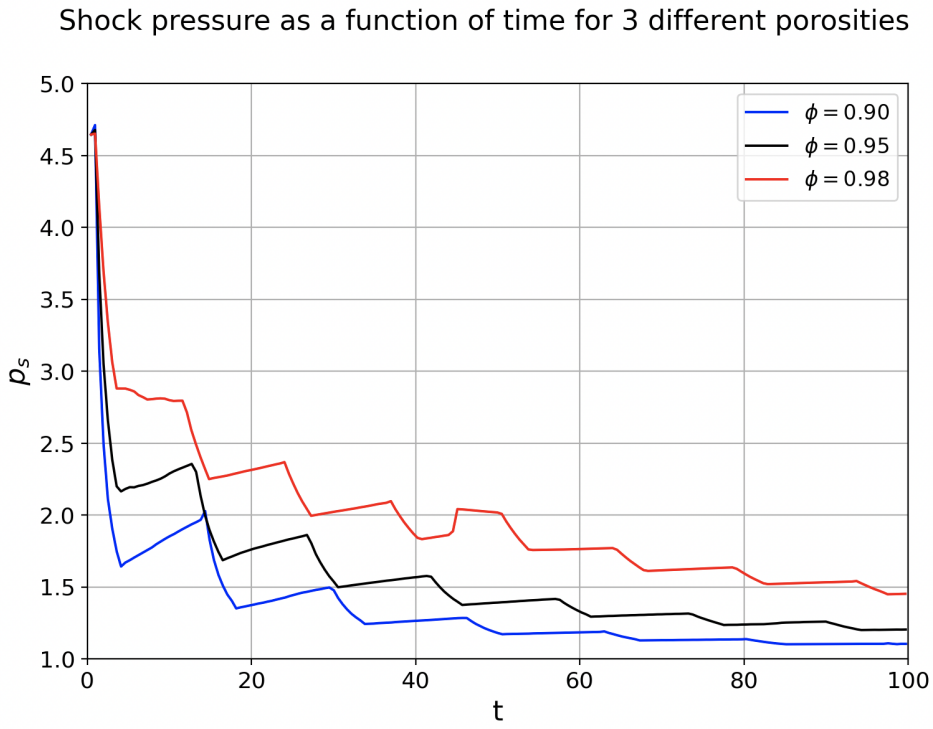

Figure 4.1: Evolution of the shock pressure p_s as a function of time for the 3 studied porosities: $\phi = 0.90$, $\phi = 0.95$ and $\phi = 0.98$. The detonation corresponds to the first termination reaction tIf1.1.

Looking at the evolution of shock pressure on this graph, it is quite clear that the detonation passes through the purely fluid and porous matrix regions over time. In fact, the decreasing zones correspond to the shock wave passing through a porous section, while the increasing zones correspond to the wave in a purely fluid region between these obstacles. This means that the distance between the reaction zone and the precursor detonation wave oscillates over the fluid/porous regions, gradually increasing until detonation quench occurs. The behavior of the three porosities is quite similar. What differs is the time-averaged pressure, which, as expected, increases with porosity. For porosities $\phi = 0.90$, $\phi = 0.95$ and $\phi = 0.98$,

respectively, we obtain average pressures of $p_{a,s_{0.90}} = 1.36$, $p_{a,s_{0.95}} = 1.58$ and finally $p_{a,s_{0.98}} = 2.00$.

This phenomenon of wave suppression is even clearer in Figure 4.2 which shows, on the one hand, the evolution of gas pressure as a function of distance and, on the other hand, the evolution of the mass fraction of reactants as a function of distance for these three different porosities. The termination reaction is also tIf1.1.

These plots confirm that detonation is correctly suppressed with this configuration, whatever the porosity analyzed here. Gas pressure is greatly reduced as it passes through a porous section (blue area on the graphs), and only slightly reduced in between. As explained in the introduction, the key factor in detonation attenuation is the interphasial force that porous obstacles exert on the reactive mixture, acting as a sink for momentum and kinetic energy. This force reduces the intensity of the shock wave, thus weakening the detonation and reducing the temperature in the reactive zone. Without this high temperature, the mixture is not rapidly consumed, resulting in a detachment between the wavefront and the reactive zone.

Some interesting points to note on some of the profiles are, firstly, the increase in pressure just in front of some obstacles, which can be seen, for example, for the time instance $t = 20$ in front of the second obstacle. This peak is in fact a shock wave that reflects off the obstacle and travels upstream in the flow. This is also the case for the time instance $t = 40$ in front of the third obstacle encountered, for all three porosities.

Finally, as a point of comparison, a similar simulation was carried out in the article "Attenuation of gaseous detonations by porous media of fine microstructure" [12]. The difference being that it was performed with the second termination reaction, tIIf1.1, for a porosity of $\phi = 0.95$. In the present configuration tIf1.1 with $\phi = 0.95$, the attenuation rate is lower and the shocks reflected by the obstacles are more pronounced. Furthermore, the article under consideration mentions that chain explosions are observed because the temperature after attenuation remains higher than the cross-over temperature T_c, thus increasing the concentration of radicals. In the present case, this phenomenon cannot be observed and may be attributed to the higher cross-over temperature T_c of the first termination reaction tIf1.1. In any case, it has been shown in this reference document that these chain explosions attenuate very quickly once a new obstacle is encountered, having very little influence on the power loss of the shock wave.

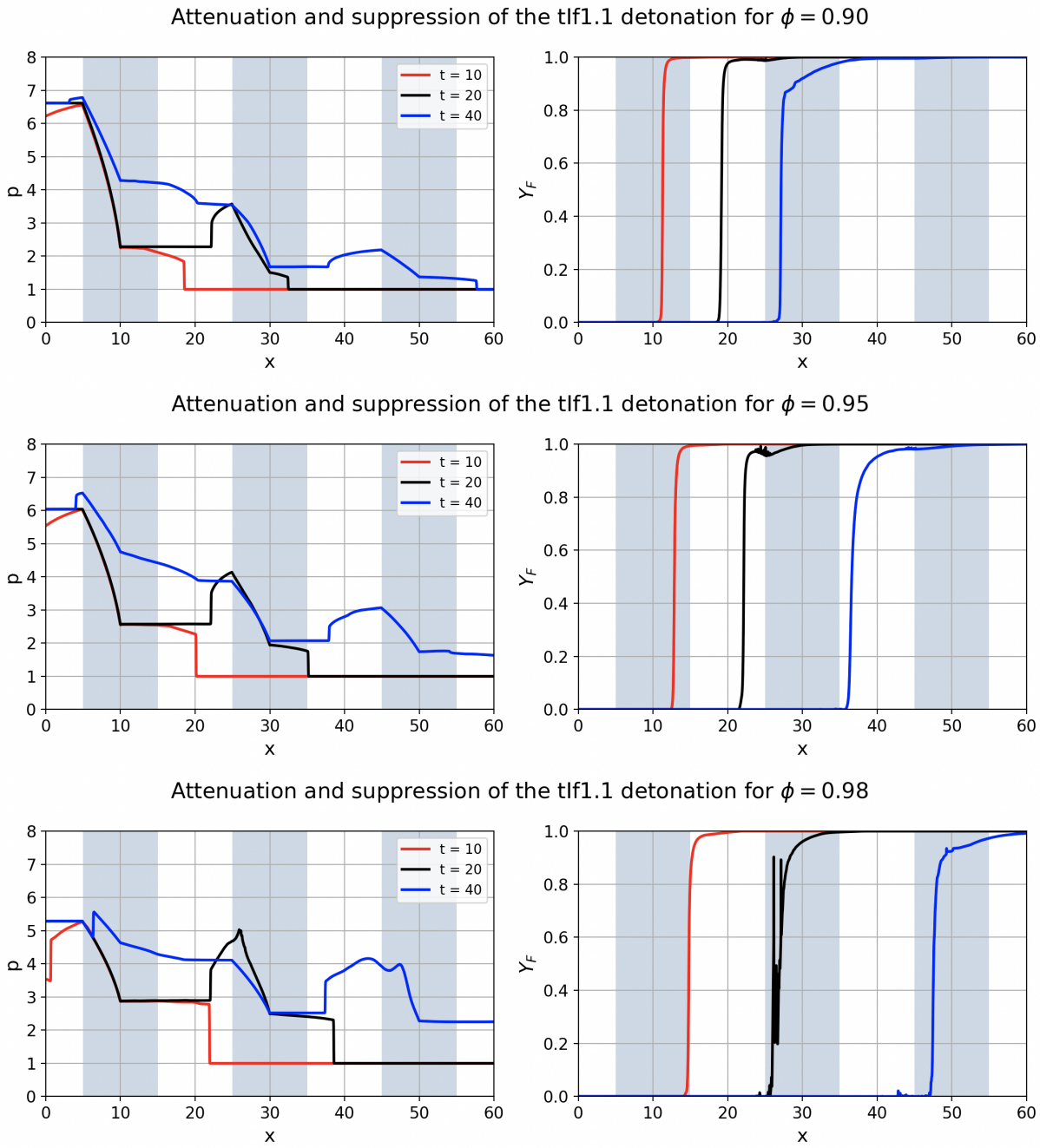

Figure 4.2: Pressure and mass fraction of reactant profiles for the tIf1.1 detonation, with 3 different porosities: $\phi = 0.90$, $\phi = 0.95$, $\phi = 0.98$. On the left column, the different pressures p and on the right column, the mass fraction of the reactants Y_F. Three time instances are shown (t=10, t=20 and t=40). The blue sections represent the porous obstacles.

4.2. Two-dimensional results

In this section, the results presented are all performed with the second tIIf1.1 termination reaction. The first configuration, comprising bi-periodically arranged blocks, is analyzed with varying porosities. The second configuration examines different wall thicknesses, also taking variable porosities into account.

4.2.1. Biperiodic array of porous blocs

This configuration is very similar to the previous one, except that the obstacles don't cover the whole section. The blocks have a thickness of $10l_{1/2}$ and a width of $5l_{1/2}$, periodically distributed every $20l_{1/2}$ and starting at $5l_{1/2}$ from the left inflow boundary. The special feature here is that the same two periods of $10l_{1/2}$ are simulated on the y axis, to obtain this biperiodic arrangement. The upper and lower limits are still defined as periodic. As before, a plot of the shock pressure p_s as a function of time is provided in Figure 4.3. The pressure profile is located at the lower limit $y = 0$, so there is no obstacle in its path.

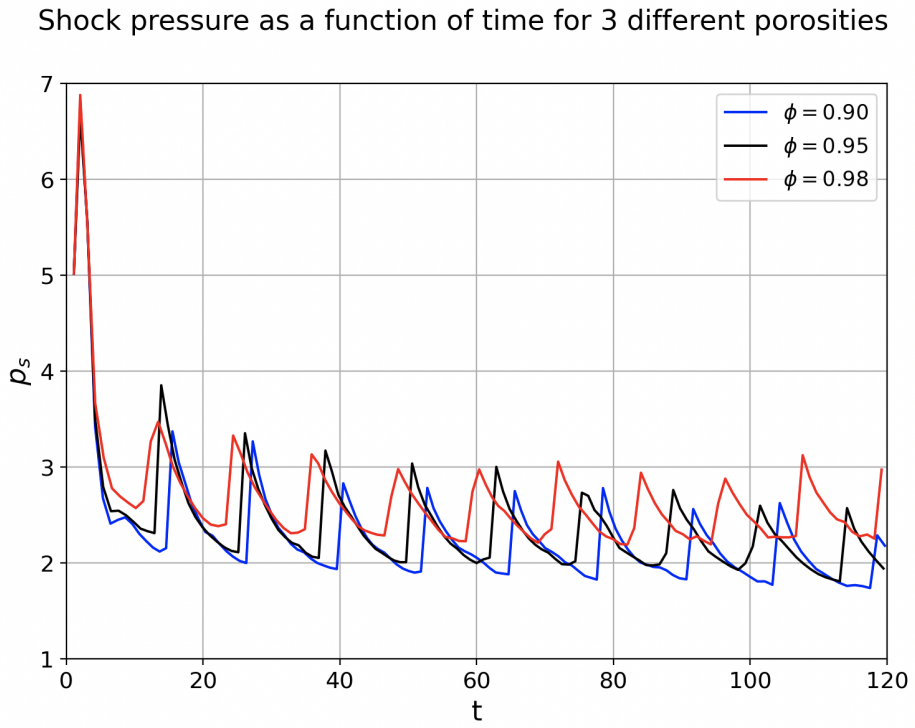

Figure 4.3: Evolution of the shock pressure p_s as a function of time at $y = 0$ for the 3 studied porosities: $\phi = 0.90$, $\phi = 0.95$ and $\phi = 0.98$. The detonation corresponds to the second termination reaction tIIf1.1.

With regard to the average shock pressure, the same behavior is observed as in 1D: the higher the porosity, the higher the average pressure. For porosities $\phi = 0.90$, $\phi = 0.95$ and $\phi = 0.98$, respectively, we obtain average pressures of $p_{a,s_{0.90}} = 2.29$, $p_{a,s_{0.95}} = 2.42$ and finally $p_{a,s_{0.98}} = 2.66$. These average pressures are much higher than in the one-dimensional case, which can be explained by the fact that the obstacles do not cover the entire cross-section, allowing the shock wave to sustain itself longer over time. In terms of the curve profile, the pressure drops drastically after the first obstacle. This is followed by an oscillating profile that lasts over time, and has approximately the same frequency for the three porosities studied here. This means that it is the configuration of the blocks, i.e. the distance between them, that dictates the amplitude and frequency of the oscillations, and not their porosity (at least between 90% and 98%).

Next, level curves for gas pressure p and reactant mass fraction Y_F are plotted for the three different porosities, with three time instances for each in Figure 4.5, Figure 4.6 and Figure 4.7. First, let's analyze the impact of porous blocks on these contours:

– *Pressure curves (gray/blue lines)*: It is possible to see two different behaviors of these curves when in a purely fluid region and when encountering an obstacle. The purely fluid case represents the typical cellular pattern of shock waves traveling in a channel, just as in Figure 4.4:

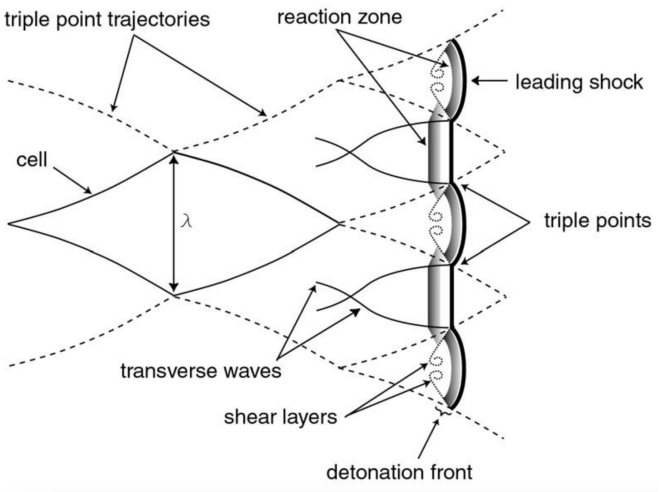

Figure 4.4: Typical pattern of a detonation moving through an open channel [45]

The wavefront is particularly curved and triple points appear. As soon as an obstacle is encountered, the wavefront flattens out and becomes almost a completely straight line. The transverse components of the main wave and those created by the triple points (see Figure 4.4) appear to be attenuated.

– *Mass fraction of reactants curves (red lines)*: The red curves furthest to the right represent the reaction front, which is supposed to be very close to the shock wave front. The reaction front appears to be considerably slowed when encountering an obstacle. Indeed, it can be seen that these curves are stretched along these blocks, presenting a very curved front between them. Upstream, the mass fraction curves are almost static within the blocks, demonstrating the effectiveness of the interphasial force imposed by these obstacles.

In all simulations, the shock wave front is at a considerable distance from the reaction front. As in the 1D configuration, the interphasial force reduces the intensity of the shock wave, thereby reducing the temperature of the reactive mixture. The mixture is consumed less rapidly, which explains this distance. But the difference is that the unobstructed parts make the detonation more sustainable: as soon as the main shock leaves an obstacle, the triple points re-form very quickly. The detonation regains strength as it passes through the pure fluid domains. In the simulations carried out, it is therefore not possible to see the suppression of detonation, even if it is strongly attenuated by the porous obstacles acting as momentum sinks.

Earlier, quasi-detonations were mentioned along with their propagation method. As a reminder, in the article by Medvedev et al. [24], the reflection of the precursor shock from the domain walls heats the unburnt material formed by the dissipation of the detonation. This accelerates the deflagration, which eventually attaches itself to the front, leading to the re-initiation of the detonation. In this case, it is more a case of low-velocity detonation, as the reaction front maintains a certain distance from the shock-wave front over time.

Finally, by comparing the three different porosities, it can be observed that the difference in shock velocity between $\phi = 0.90$ and $\phi = 0.95$ is not that large. In fact, the shock velocity difference between $\phi = 0.95$ and $\phi = 0.98$ is greater, as can be seen in Table 4.1.

Detonation speed averaged on time		
Configuration	Detonation speed D	% of the initial detonation speed
tIIf1.1 ; $\phi = 0.90$	1.49	65 %
tIIf1.1 ; $\phi = 0.95$	1.57	69 %
tIIf1.1 ; $\phi = 0.98$	1.70	75 %

Table 4.1: Comparison of the detonation speed for the three different porosities

The reason is that as ϕ decreases, the detonation attenuation rate reaches a

plateau. This means that the detonation velocity D reaches its minimum at relatively high values of ϕ, making the variation in D more significant when ϕ goes from 0.98 to 0.95 than when it goes from 0.95 to 0.90.

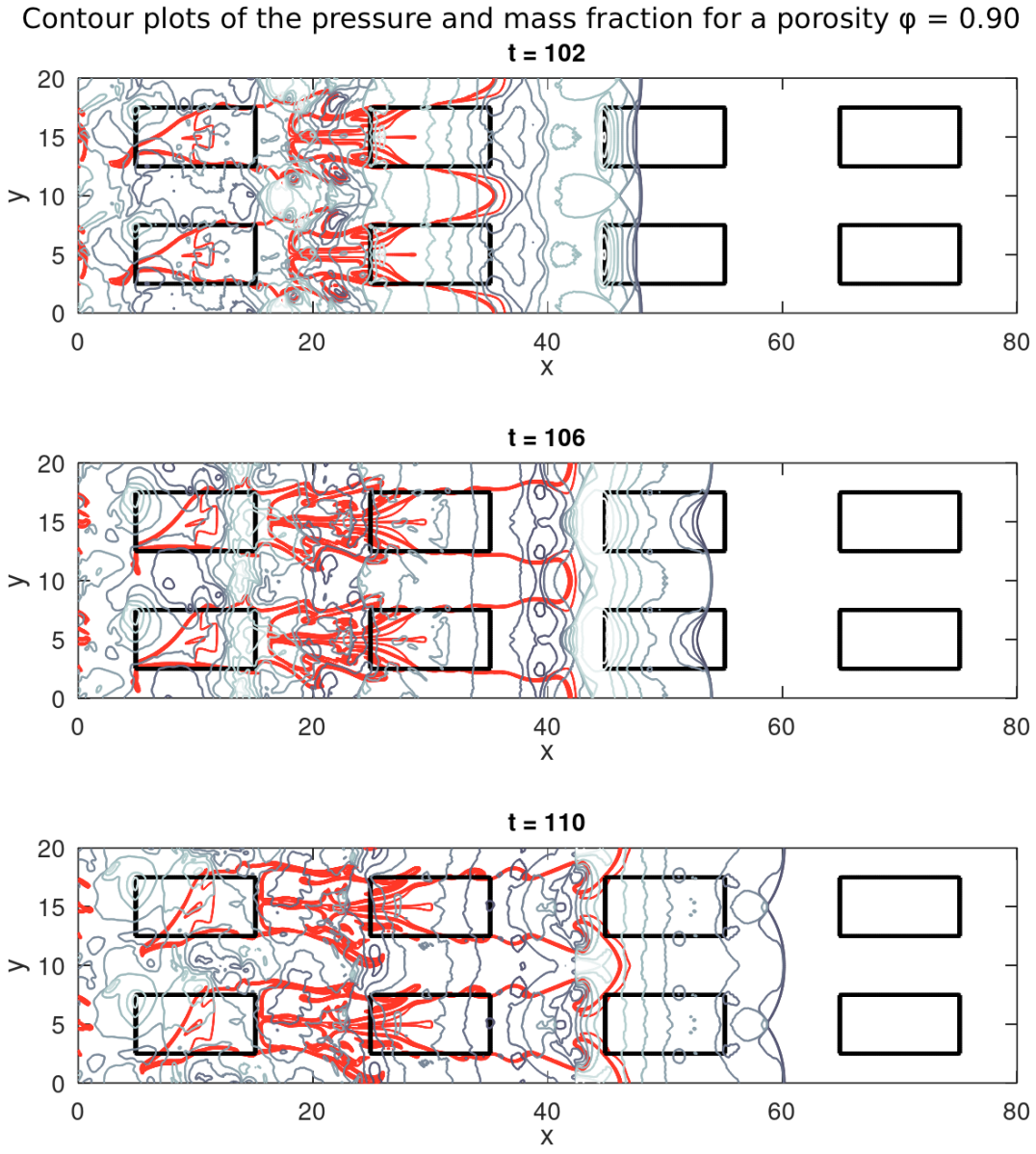

Figure 4.5: Pressure and mass fraction contour plot for the tIIf1.1 detonation, in a bi-periodic configuration with a porosity of $\phi = 0.90$. The red lines correspond to the mass fraction of the reactants Y_F, and the gray/blue lines to the pressure p. Three time instances are shown (t=102, t=106 and t=110).

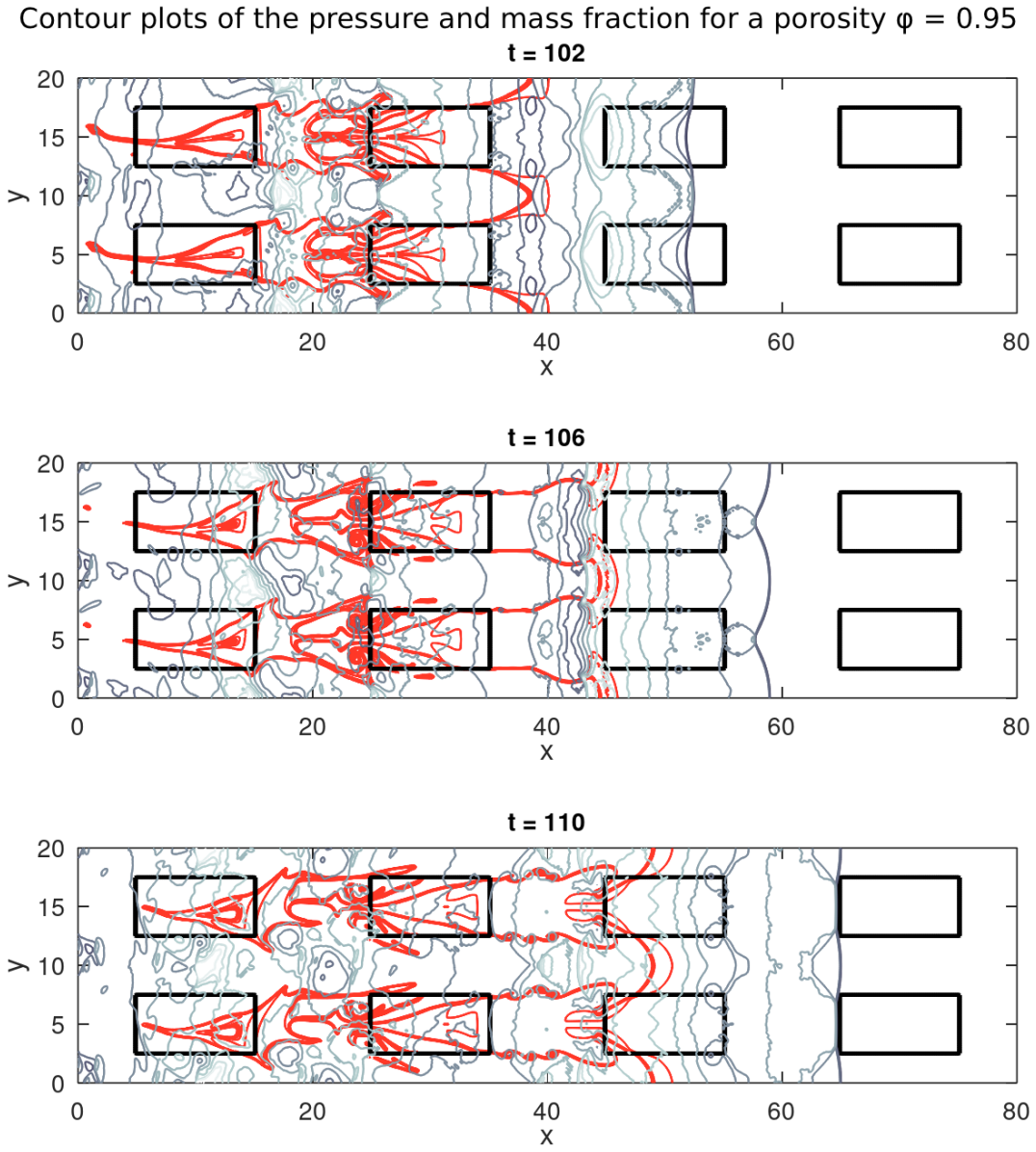

Figure 4.6: Pressure and mass fraction contour plot for the tIIf1.1 detonation, in a bi-periodic configuration with a porosity of $\phi = 0.95$. The red lines correspond to the mass fraction of the reactants Y_F, and the gray/blue lines to the pressure p. Three time instances are shown (t=102, t=106 and t=110).

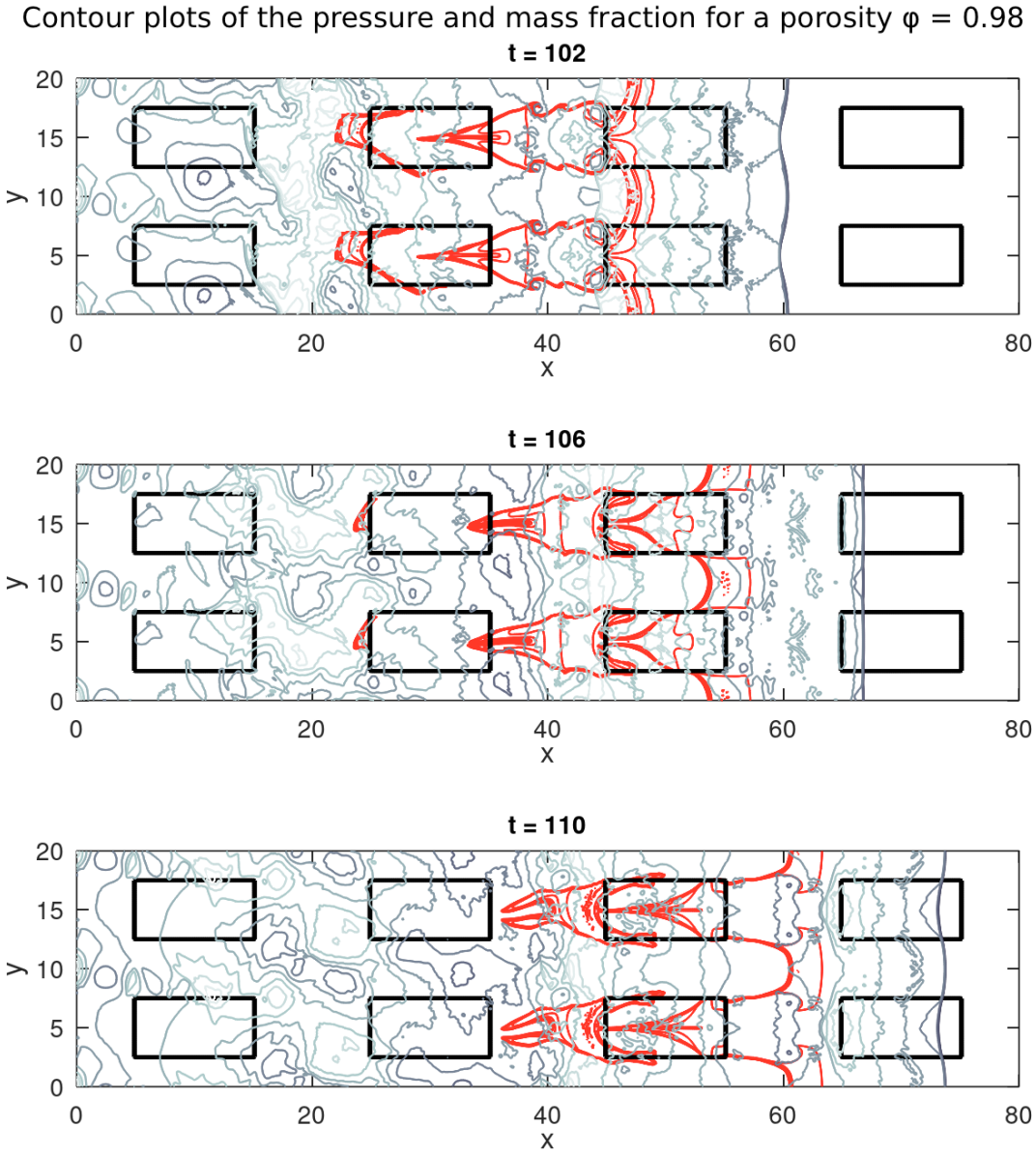

Figure 4.7: Pressure and mass fraction contour plot for the tIIf1.1 detonation in a bi-periodic configuration, with a porosity of $\phi = 0.98$. The red lines correspond to the mass fraction of the reactants Y_F, and the gray/blue lines to the pressure p. Three time instances are shown (t=102, t=106 and t=110).

4.2.2. Porous coatings on the walls

This configuration is composed of a thickness of porous medium along the entire length of the domain. Two thicknesses are studied here: $2.5l_{1/2}$ and $5.0l_{1/2}$ with porosities $\phi = 0.90$ and $\phi = 0.95$. As with biperiodic obstacles, only the tllf1.1 reaction is analyzed. However, this time, the upper and lower boundaries are set to reflecting wall conditions.

It seems that detonation tends to quench here. Indeed, it is very noticeable that the distance between the shock wave front and the reaction front increases over time for all the cases studied in Figure 4.8, Figure 4.9, Figure 4.10 and Figure 4.11. The behavior for both porosities in the $2.5l_{1/2}$ wall thickness configuration is the same. The distance between the shock front and the reaction increases from $6.5l_{1/2}$ at time $t = 20$ to $10l_{1/2}$ at time $t = 36$, and continues to increase over time. The same applies to the wall thickness $5l_{1/2}$ for both porosities. Despite this, as expected, the case with the thicker $5l_{1/2}$ coating (Figure 4.10 and Figure 4.11) has a higher detonation attenuation rate, which is due to the greater interphasial force. Simulations of this configuration with the first tIf1.1 termination reaction have also been carried out, but they show no specific interest given the similarity of the results. The same applies to analyses with a porosity of $\phi = 0.98$.

As for the pressure curves (gray/blue curves), the wave front is clearly discernible with its curvature, and occupies the entire width of the domain. The reactant mass fraction curves (red curves) evolve in the unobstructed part, and are strongly slowed down in the porous walls thanks to the interphasial force. The slowdown is particularly marked in the porous lateral section, where the curves are stretched outwards. In Figure 4.10, i.e. the $5l_{1/2}$ thickness case with a porosity of $\phi = 0.90$, we can see that the wavefront is more curved than in the other cases. Furthermore, at the upper and lower limits, we notice that the wavefront is no longer the full width of the channel, which may be due to the attenuation of the lateral components, caused by a higher interphasial force in this case.

As already mentioned in the state of the art, G. Y. Bivol et al. have experimentally studied "Detonation suppression in hydrogen-air mixture using porous coatings on the walls" [30]. These coatings include polyurethane foam and metal wool, with porosities quite similar to the present case: between 95% and 99%. They concluded that "the decoupling of the detonation wave into a shock wave and flame front was observed in the porous section of the detonation tube with both materials". Numerical and experimental results therefore support the decoupling of the shock wave, which ultimately leads to its quenching.

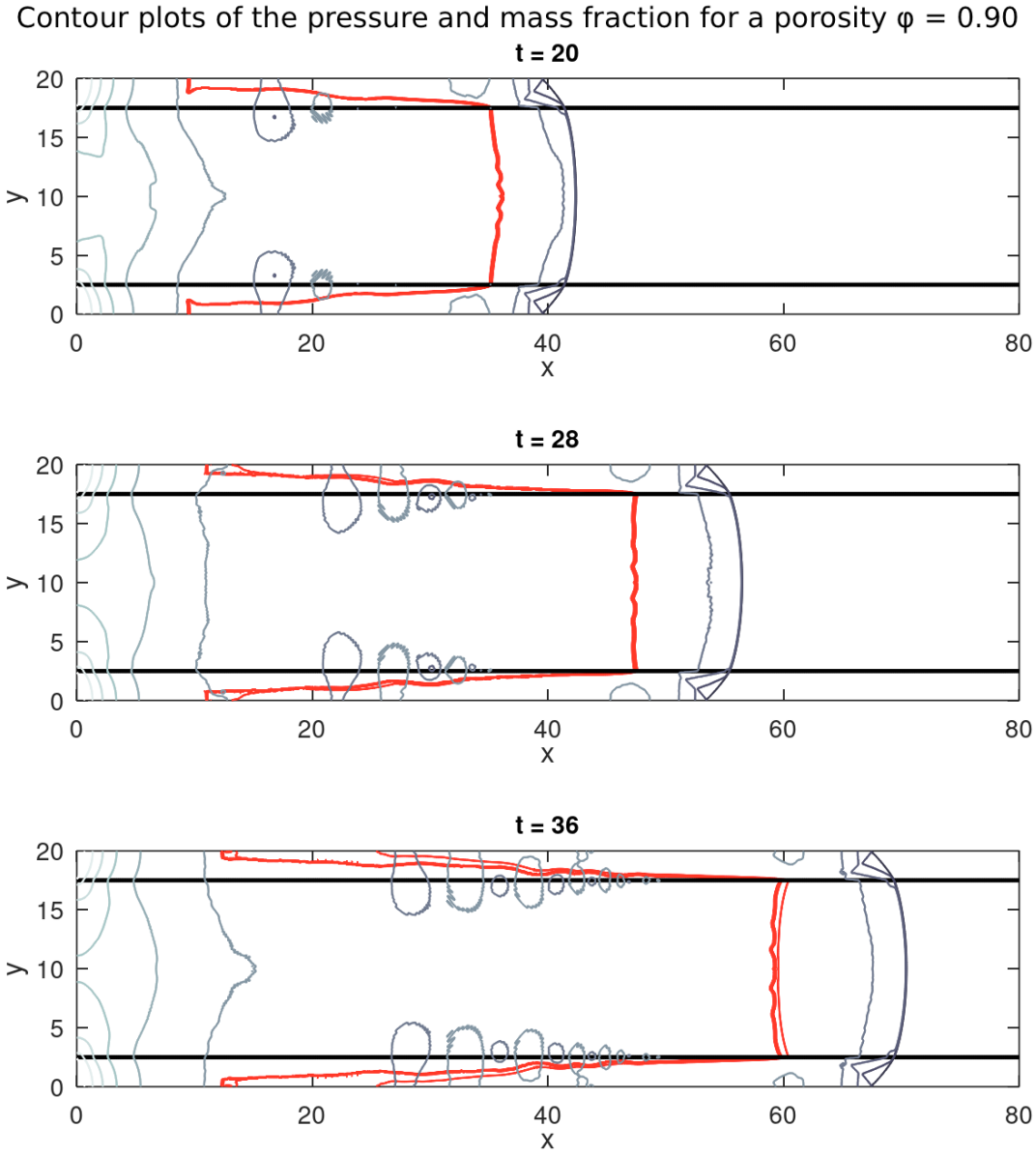

Figure 4.8: Pressure and mass fraction contour plot for the tIIf1.1 detonation, in a porous wall configuration ($2.5l_{1/2}$ width) with a porosity of $\phi = 0.90$. The red lines correspond to the mass fraction of the reactants Y_F, and the gray/blue lines to the pressure p. Three time instances are shown (t=20, t=28 and t=36).

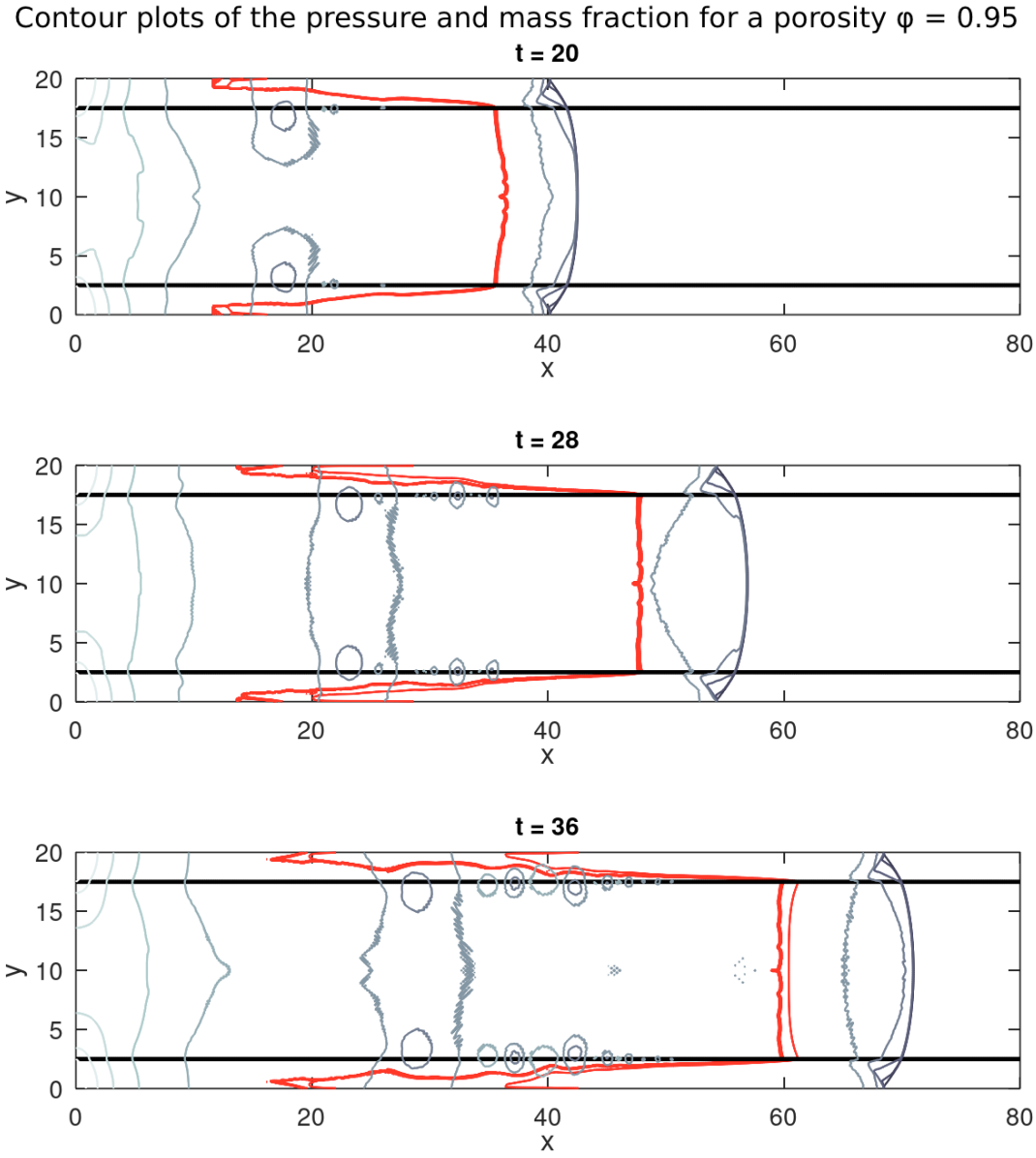

Figure 4.9: Pressure and mass fraction contour plot for the tIIf1.1 detonation, in a porous wall configuration ($2.5l_{1/2}$ width) with a porosity of $\phi = 0.95$. The red lines correspond to the mass fraction of the reactants Y_F, and the gray/blue lines to the pressure p. Three time instances are shown (t=20, t=28 and t=36).

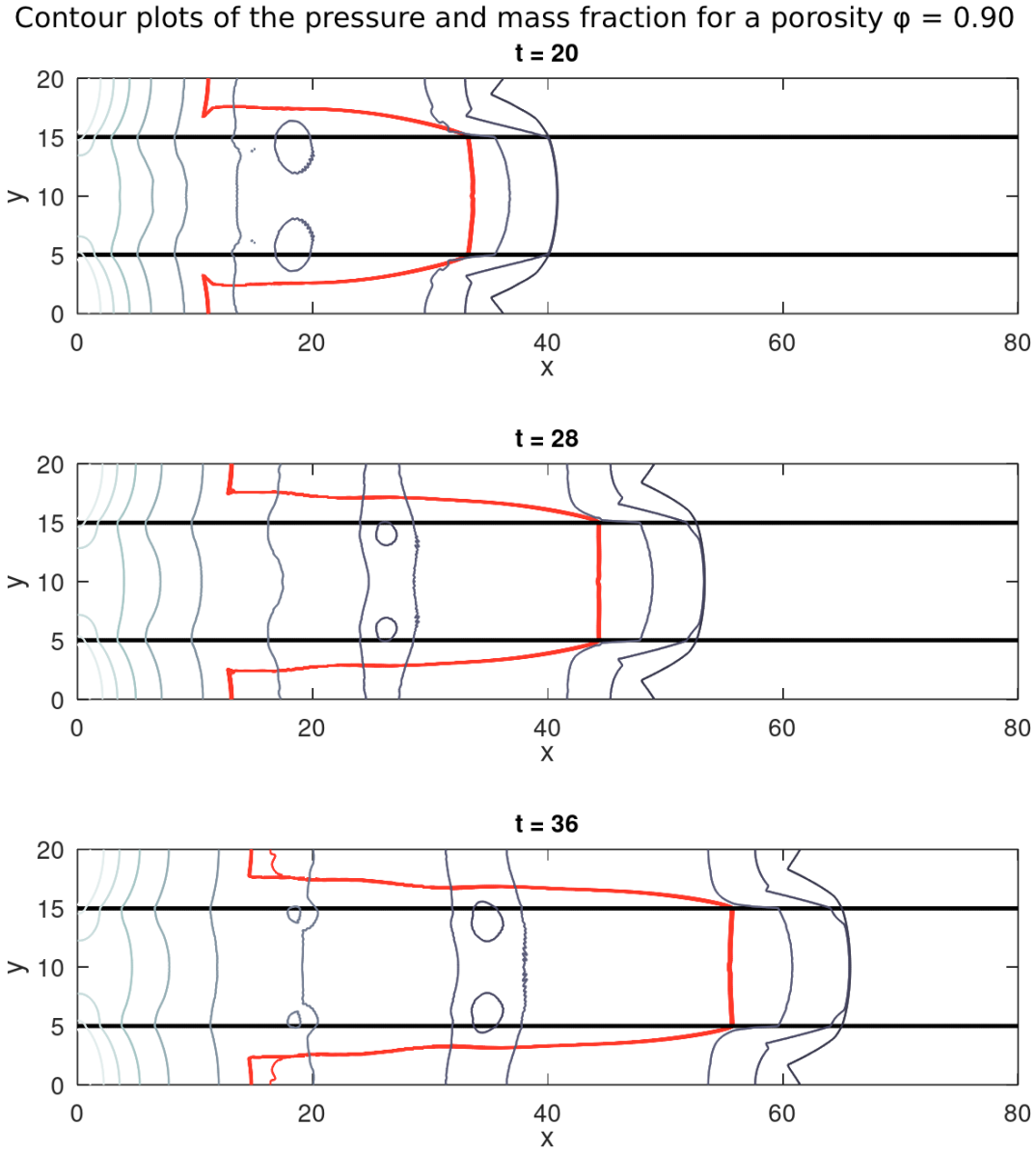

Figure 4.10: Pressure and mass fraction contour plot for the tIIf1.1 detonation, in a porous wall configuration ($5l_{1/2}$ width) with a porosity of $\phi = 0.90$. The red lines correspond to the mass fraction of the reactants Y_F, and the gray/blue lines to the pressure p. Three time instances are shown (t=20, t=28 and t=36).

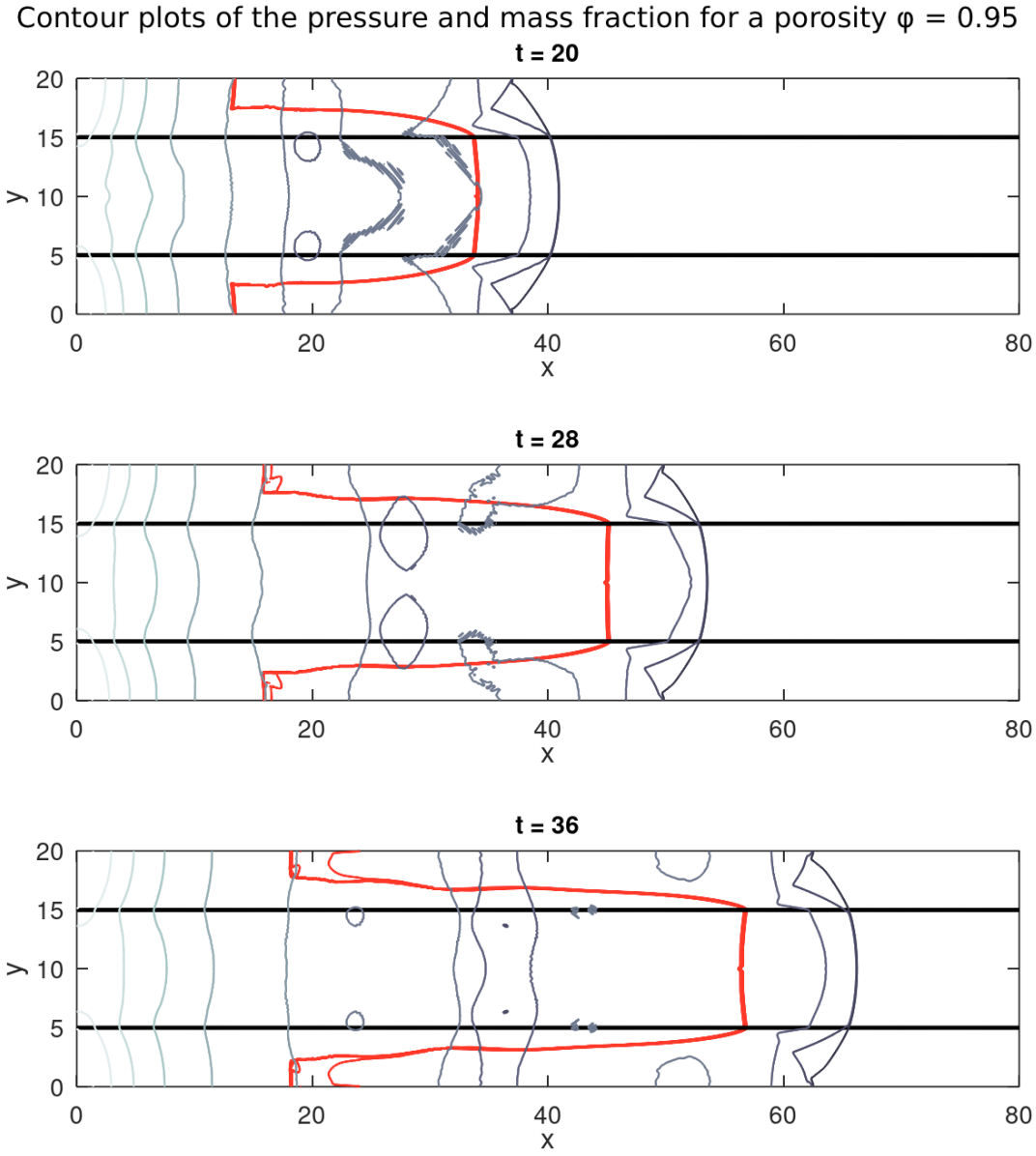

Figure 4.11: Pressure and mass fraction contour plot for the tIIf1.1 detonation, in a porous wall configuration ($5l_{1/2}$ width) with a porosity of $\phi = 0.95$. The red lines correspond to the mass fraction of the reactants Y_F, and the gray/blue lines to the pressure p. Three time instances are shown (t=20, t=28 and t=36).

Finally, the temperature profile inside ($y = 0$) and outside ($y = 10$) the porous medium are shown in Figure 4.12. These temperature profiles support the observations made above. In the coating ($y = 0$), the temperature is just below the cross-over temperature $T_c = 1.27$ throughout the length. It confirms again that the coating is effective in attenuating the detonation, since the interphasial force slows the combustion front, thus reducing the temperature. In the free region, we can see that the shock temperature (steep decreasing to $T = 1$) is lower than the cross-over temperature T_c. Combustion begins when $T > T_c$, which is clearly seen in the graph with a sharp increase in temperature. We can also see very clearly that the distance between the shock front and the combustion zone increases with time, looking at the case of the free region.

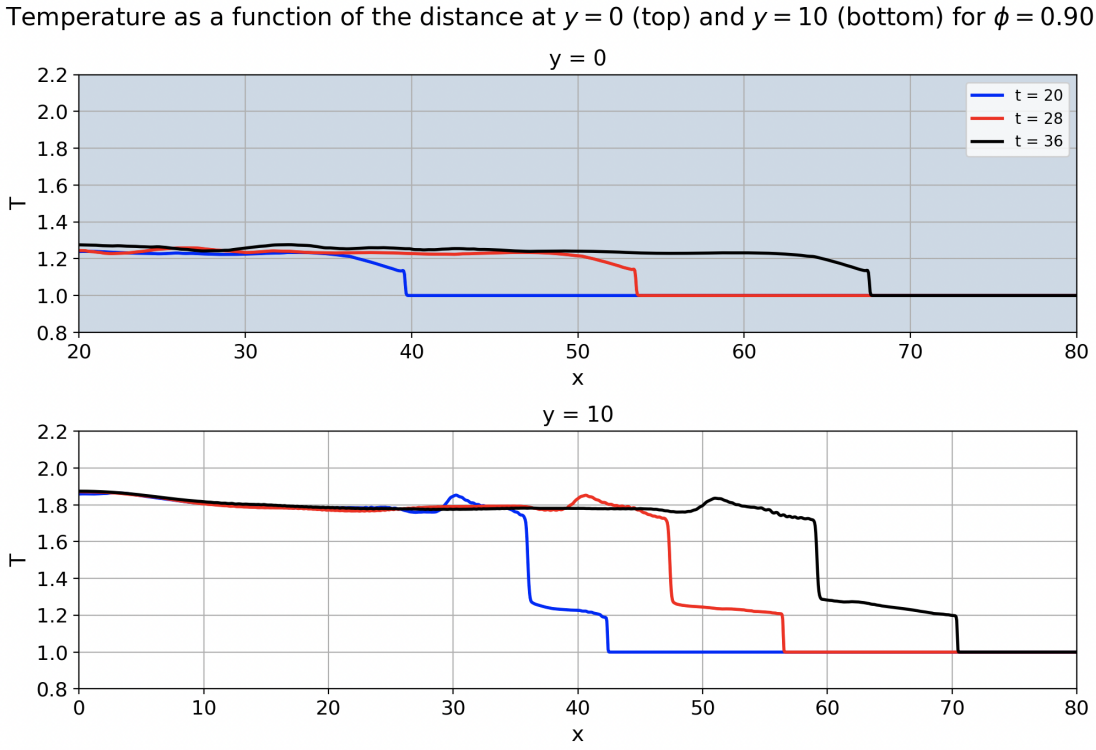

Figure 4.12: Temperature as a function of distance for the tIIf1.1 detonation in a porous coating walls ($2.5l_{1/2}$) configuration, with a porosity of $\phi = 0.90$. On the top, $y = 0$ (into the porous medium); At the bottom, $y = 10$ (In the middle if the channel). The blue sections represent the porous coating.

5 Conclusion

In this master's thesis, a numerical analysis of accidental detonation suppression was carried out for different configurations of porous obstacles in a channel. This was performed using a FORTRAN algorithm and program developed by Prof. Papalexandris' research team. It is based on a thermomechanical model for superimposed fluid/porous regions. The gas-phase equilibrium equations are solved using a shock-capturing algorithm for hyperbolic conservation laws with source terms. On the other hand, the equilibrium equation for the porous phase is solved using a more conventional method, which is none other than a second-order Runge-Kutta (RK2) solver.

In this model, the porous medium is considered as a rigid, inert, velocity-free solid with a constant mass density. This medium is the key to the attenuation mechanism, since it exerts a force on the reactive mixture, acting as a sink of kinetic energy and momentum. In addition, two chemical kinetics were taken into account, with two different termination reactions: one more suited to high pressures, and the other to moderate and low pressures.

More specifically, the interest of this study was to assess the effectiveness of the attenuation mechanism, in order to know whether or not detonation is suppressed. To this end, the main element examined was the porosity ϕ with several configurations of obstacles in one and two dimensions.

In one dimension, a network of periodic obstacles covering the entire cross-section effectively suppresses tIf1.1 detonation for all porosities studied. The distance between the shock wave front and the reaction zone increases obstacle by obstacle, resulting in increasing ignition delay. The result is a decoupling of the detonation, which eventually disappears.

In two dimensions, a biperiodic network of obstacles not covering the entire cross-section does not confirm that the shock is indeed suppressed. In this case, the shock wave is able to maintain itself longer, with a significant distance between the shock wave front and the reaction zone. This may appear to be a quasi-detonation profile, as explained in the Medvedev et al. article [24], but in reality, the wave does not re-initiate. The result is a low-velocity detonation. Finally, it is possible to observe that the detonation velocity reaches a "minimum" for decreasing porosity values. Indeed, as porosity decreases, the attenuation rate of detonation reaches a plateau.

Last but not least, a porous coating can also effectively suppress detonation, and quite quickly. As might be expected, a greater thickness of the porous medium attenuates detonation more effectively, because of the greater interphasial force. The experimental results of Bivol et al. [30] agree with the results presented here in which detonation is decoupled into a shock wave and a flame front, giving a clearer idea of the types of porous materials that can be used in real applications.

Although the simulations carried out provide an advance on the attenuation efficiency of porous objects in different configurations, some key parameters could be adjusted to explore a wider range of detonation scenarios.

- *Overdrive factor* f : As the overdrive factor increases, the shock wave becomes stronger, leading to rapid compression and heating of the reactants. This can potentially lead to more complete and efficient combustion. Secondly, this factor also affects detonation stability. A highly overdriven detonation will tend to be more stable. It is therefore possible to test a wider range of this factor in order to extend the research and compare the conclusions already obtained. M. Papalexandris has already explored a special case with an overdrive factor of $f = 1.6$ [12]. He confirms that the shock is stronger and that the re-initiation time after crossing a single obstacle is shorter than with $f = 1.1$. Further study of this parameter could bring interesting data to these simulations.

- *Heat of combustion* q : Another interesting parameter to investigate is the heat of combustion. The latter directly influences the amount of energy released during a detonation. Testing other values would mean taking into account other mixture compositions, which may also be of interest in the context of this study.

Finally, integrating 3D simulations could bring a number of significant advantages and a deeper insight into what 1D and 2D simulations can offer.

- Detonations are subject to numerous transverse instabilities, which induce variations in pressure and temperature. As a result, the mixture does not react uniformly throughout the domain, which can affect propagation velocity, detonation wave direction, etc. 3D simulations can capture these more complex and realistic flow structures, for a better understanding of their behavior.

- The 3D configuration of porous obstacles can lead to complex flow trajectories due to their walls and corners. There may be shock interactions that are not taken into account in 1D or 2D. As a result, the shape, orientation and spacing of obstacles will have a greater influence, leading to more accurate results.

- Finally, these 3D simulations can be used to generate real-life simulations, with configurations, porosities or even mixtures that may correspond to actual cases of industrial installations, for example.

Bibliography

[1] M. V. Papalexandris, *Gas Dynamics*. PUL Presses Universitaires de Louvain, 2022.

[2] C.-Y. Wen, Y. Jiang, and L. Shi, "Space–time conservation element and solution element method," in Springer, 2023, pp. 95–122.

[3] A. Minchinton, "On the influence of fundamental detonics on blasting practice," *Conference Paper*, 2015.

[4] D. L. Chapman, "On the rate of explosions in gases," *Philos. Mag.*, 47:90–104, 1899.

[5] E. Jouguet, "On the propogation of chemical reaction in gases," *J. de Mathematiques Pures et Appliques*, 7:347–425, 1905.

[6] J. Shepherd, "Detonation in gases," *In Proceedings of the Combustion Institute, Volume 32, Issue 1*, pp. 83–96, 2009.

[7] Y. B. Zeldovich, *On the theory of the propagation of detonation in gaseous systems*. 1950.

[8] J. V. Neuman, "Theory of detonation waves," *Institute for Advanced Study, Princeton, NJ*, 1942.

[9] W. Döring, "On detonation process in gases," *Ann. Phys. 43 - 9*, 1943.

[10] S. Kumar, M. Nehra, D. Kedia, N. Dilbaghi, K. Tankeshwar, and K.-H. Kim, "Nanodiamonds: Emerging face of future nanotechnology," in Carbon, Volume 143, 2019, pp. 678–699.

[11] P. V. Bulata and K. N. Volkov, "Detonation jet engine. part ii – construction features," in International Journal Of Environmental Science Education, 2016, pp. 5020–5033.

[12] M. V. Papalexandris, "Attenuation of gaseous detonations by porous media of fine microstructure," *Combustion and flame, Vol. 232*, 2021.

[13] I. O. Moen *et al.*, "The influence of diluents and inhibitors on detonations," in Proceedings Combustion Institute, Volume 20, Issue 1, 1985, pp. 1717–1725.

[14] F. Evariste, M. Lefebvre, and P. J. V. Tiggelen, "Inhibition of detonation wave with halogenated compounds," in Shoch Waves 6, 1996, pp. 233–239.

[15] M. V. Papalexandris, "Numerical study of detonation transmission in mixtures containing chemical inhibitors," *Physics of Fluids 24*, 2012.

[16] B. Zhang, N. Mehrjoo, H. D. Ng, J. H. Lee, and C. Bai, "On the dynamic detonation parameters in acetylene–oxygen mixtures with varying amount of argon dilution," in Combustion and flame 161, 2014, pp. 1390–1397.

[17] M. Papalexandris, J. Thomas, C. Jacobs, and V. Deledicque, "Structural characteristics of detonation expansion from a small channel to a larger one," in Proceedings of the Combustion Institute, Volume 31, 2007, pp. 2407–2414.

[18] F. Pintgen and J. Shepherd, "Detonation diffraction in gases," in Combustion and flame 156, 2009, pp. 665–677.

[19] R. Sorin, R. Zitoun, B. Khasainov, and D. Desbordes, "Detonation diffraction through different geometries," in Shock Waves 19, 2009, pp. 11–23.

[20] M. Arienti and J. E. Shepherd, "A numerical study of detonation diffraction," in J. Fluid Mech. 529, 2005, pp. 117–146.

[21] V. Guilly, "Etude de la diffraction de la détonation des mélanges $C2H2/O2$ stoechiometriques dilues par l'argon," Ph.D. dissertation, Université de Poitiers, 2005.

[22] J.-P. Dionne, H. D. NG, and J. H. S. Lee, "Transient development of friction-induced low-velocity detonations," in Proceedings of the Combustion Institute, Volume 28, 2000, pp. 645–651.

[23] I. Brailovskya and G. Sivashinsky, "Hydraulic resistance and multiplicity of detonation regimes," in Combustion and Flame, Volume 122, 2000, pp. 130–138.

[24] S. P. Medvedev, S. V. Khomik, and B. E. Gel'fand, "Recovery and suppression of the detonation of hydrogen-air mixtures at an obstacle with orifices," in Russian Journal of Physical Chemistry B, Volume 3, 2009, pp. 963–970.

[25] A. Teodorczyk, J. Lee, and R. Knystautas, "Propagation mechanism of quasi-detonations," in Symposium (International) on Combustion, Volume 22, Issue 1, 1989, pp. 1723–1731.

[26] G. A. Lyamin, "Heterogeneous detonation in a rigid porous medium," in Combustion, Explosion and Shock Waves, Volume 20, 1984, pp. 719–722.

[27] C. Kauffman, C. Yan, and J. Nicholls, "Gaseous detonations in porous media," in Symposium (International) on Combustion, Volume 19, Issue 1, 1982, pp. 591–597.

[28] T. Slungaard, T. Engebretsen, and O. Sønju, "The influence of detonation cell size and regularity on the propagation of gaseous detonations in granular materials," in Shock Waves, Volume 12, 2003, pp. 301–308.

[29] M. Radulescu and B. M. N. Maxwell, "The mechanism of detonation attenuation by a porous medium and its subsequent re-initiation," in J. Fluid Mech., vol. 667, 2011, pp. 96–134.

[30] G. Y. Bivol, S. V. Golovastov, and V. V. Golub, "Detonation suppression in hydrogen–air mixtures using porous coatings on the walls," in Shock Waves, Volume 28, 2018, pp. 1011–1018.

[31] G. Y. Bivol and S. V. Golovastov, "Effects of polyurethane foam on the detonation propagation in stoichiometric hydrogen-air mixture," in Process Safety and Environmental Protection, Volume 130, 2019, pp. 14–21.

[32] G. Y. Bivol, S. V. Golovastov, and V. V. Golub, "Effects of the pore size on hydrogen–air detonation propagation in the channel with porous walls," in Journal of Physics: Conference Series, Vol. 1147, 2019.

[33] M. Papalexandris and P. Antoniadis, "A thermo-mechanical model for flows in superposed porous and fluid layers with interphasial heat and mass exchange," in International Journal of Heat and Mass Transfer, Vol. 88, 2015, pp. 42–55.

[34] M. Papalexandris, "A two-phase model for compressible granular flows based on the theory of irreversible processes," in Journal of Fluid Mechanics 517, 2004, pp. 103–112.

[35] D. Systems, *Isotropic and orthotropic materials*, `https://help.solidworks.com/2024/english/SolidWorks/cworks/c_isotropic_orthotropic_materials.htm?verRedirect=1`, Accessed on 2024-06-11.

[36] V. Deledicque and M. V. Papalexandris, "An exact riemann solver for compressible two-phase flow models containing non-conservative products," in Journal of Computational Physics, Volume 222, Issue 1, 2007, pp. 217–245.

[37] M. Short and J. Dold, "Linear stability of a detonation wave with a model three-step chain-branching reaction," in Mathematical and Computer Modelling, Volume 24, Issue 8, 1996, pp. 115–123.

[38] M. V. Papalexandris, *Combustion and Fuels*. PUL Presses Universitaires de Louvain, 2020.

[39] M. V. Papalexandris, A. Leonard, and P. E. Dimotakis, "Unsplit schemes for hyperbolic conservation laws with source terms in one space dimension," in Journal of Computational Physics, Volume 134, Issue 1, 1997, ch. 31-61.

[40] M. V. Papalexandris, A. Leonard, and P. E. Dimotakis, "Unsplit algorithms for multidimensional systems of hyperbolic conservation laws with source terms," in Computers Mathematics with Applications, Volume 44, Issues 1–2, 2002, ch. 25-49.

[41] M. Short and J. J. Quirk, "On the nonlinear stability and detonability limit of a detonation wave for a model three-step chain-branching reaction," in Journal of Fluid Mechanics, Volume 339, Issue 1, 1997, pp. 89–119.

[42] F. Sonnenwald, V. Stovin, and I. Guymer, "Estimating drag coefficient for arrays of rigid cylinders representing emergent vegetation," in Journal of Hydraulic Research, 2018, ch. 591-597.

[43] T. L. Bergman, A. S. Lavine, F. P. Incropera, and D. P. DeWitt, *Fundamentals of Heat and Mass Transfer, 8th Edition*. Wiley, 2018.

[44] idealsimulations, *Courant number*, `https://www.idealsimulations.com/resources/courant-number-cfd/`, Accessed on 2024-06-14.

[45] J. H. S. Lee, "Dynamic parameters of gaseous detonations," in Annual Review of Fluid Mechanics Volume 16, 1984, ch. 311-336.

UNIVERSITÉ CATHOLIQUE DE LOUVAIN
École polytechnique de Louvain
Rue Archimède, 1 bte L6.11.01, 1348 Louvain-la-Neuve, Belgique | **www.uclouvain.be/epl**